

A process-based analysis of ocean heat uptake in an AOGCM with an eddy-permitting ocean component

Article

Accepted Version

Kuhlbrodt, T. ORCID: <https://orcid.org/0000-0003-2328-6729>, Gregory, J. ORCID: <https://orcid.org/0000-0003-1296-8644> and Shaffrey, L. ORCID: <https://orcid.org/0000-0003-2696-752X> (2015) A process-based analysis of ocean heat uptake in an AOGCM with an eddy-permitting ocean component. *Climate Dynamics*, 45 (11). pp. 3205-3226. ISSN 1432-0894 doi: <https://doi.org/10.1007/s00382-015-2534-0> Available at <https://centaur.reading.ac.uk/39329/>

It is advisable to refer to the publisher's version if you intend to cite from the work. See [Guidance on citing](#).

To link to this article DOI: <http://dx.doi.org/10.1007/s00382-015-2534-0>

Publisher: Springer

All outputs in CentAUR are protected by Intellectual Property Rights law, including copyright law. Copyright and IPR is retained by the creators or other copyright holders. Terms and conditions for use of this material are defined in the [End User Agreement](#).

www.reading.ac.uk/centaur

CentAUR

Central Archive at the University of Reading

Reading's research outputs online

Climate Dynamics manuscript No.
(will be inserted by the editor)

1 **A process-based analysis of ocean heat uptake in an AOGCM**
2 **with an eddy-permitting ocean component**

3 **T. Kuhlbrodt · J. M. Gregory · L. C. Shaffrey**

4
5 Received: date / Accepted: date

6 **Abstract** About 90% of the anthropogenic increase in heat stored in the climate system
7 is found the oceans. Therefore it is relevant to understand the details of ocean heat up-
8 take. Here we present a detailed, process-based analysis of ocean heat uptake (OHU) pro-
9 cesses in HiGEM1.2, an atmosphere-ocean general circulation model (AOGCM) with an
10 eddy-permitting ocean component of $1/3^\circ$ resolution. Similarly to various other models,
11 HiGEM1.2 shows that the global heat budget is dominated by a downward advection of heat
12 compensated by upward isopycnal diffusion. Only in the upper tropical ocean do we find
13 the classical balance between downward diapycnal diffusion and upward advection of heat.
14 The upward isopycnal diffusion of heat is located mostly in the Southern Ocean, which thus
15 dominates the global heat budget. We compare the responses to a $4xCO_2$ forcing and an en-
16 hancement of the windstress forcing in the Southern Ocean. This highlights the importance
17 of regional processes for the global ocean heat uptake. These are mainly surface fluxes and
18 convection in the high latitudes, and advection in the Southern Ocean mid-latitudes. Changes
19 in diffusion are less important. In line with the CMIP5 models, HiGEM1.2 shows a band
20 of strong OHU in the mid-latitude Southern Ocean in the $4xCO_2$ run, which is mostly ad-
21 vective. By contrast, in the high-latitude Southern Ocean regions it is the suppression of
22 convection that leads to OHU. In the enhanced windstress run, convection is strengthened
23 at high Southern latitudes, leading to heat loss, while the magnitude of the OHU in the
24 Southern mid-latitudes is very similar to the $4xCO_2$ results. Remarkably, there is only very
25 small global OHU in the enhanced windstress run. The wind stress forcing just leads to a
26 redistribution of heat. We relate the ocean changes at high southern latitudes to the effect of
27 climate change on the Antarctic Circumpolar Current (ACC). It weakens in the $4xCO_2$ run
28 and strengthens in the wind stress run. The weakening is due to a narrowing of the ACC,
29 caused by an expansion of the Weddell Gyre, and a flattening of the isopycnals, which are
30 explained by a combination of the wind stress forcing and increased precipitation.

T. Kuhlbrodt, J. M. Gregory and L. C. Shaffrey
NCAS, Department of Meteorology
University of Reading
Earley Gate, PO Box 243
Reading RG6 6BB, UK E-mail: t.kuhlbrodt@reading.ac.uk

J. M. Gregory
Met Office Hadley Centre
Exeter, UK

31 **Keywords** Ocean heat uptake · Process-based analysis · Advection-diffusion balance ·
32 Isopycnal diffusion · Eddy-permitting ocean model · Southern Ocean · Antarctic
33 Circumpolar Current

34 1 Introduction

35 Ocean heat uptake leads to thermal expansion of the sea water, which is one of the main
36 causes of sea level rise globally (Church et al, 2011). Therefore, understanding ocean heat
37 uptake (OHU) processes helps to reduce the large uncertainty exhibited by contemporary cli-
38 mate models in projections of future sea level change, especially on regional scales (Yin et al,
39 2010; Pardaens et al, 2011; Yin, 2012; Bouttes et al, 2012). Due to a lack of process-based
40 observations with a global coverage, models are valuable for the analysis of ocean heat up-
41 take processes. On a global scale, Gregory and Forster (2008) and Dufresne and Bony (2008)
42 analysed the spread of atmosphere-ocean general circulation models (AOGCMs; used for the
43 Coupled Model Intercomparison Project 3 [CMIP3]) in terms of ocean heat uptake under an
44 idealized CO₂ increase, however without analysing the OHU processes in detail. Kuhlbrodt
45 and Gregory (2012) similarly analysed the CMIP5 models. They found that most models
46 have a vertical temperature gradient that is too weak, suggesting an over-estimate of ocean
47 heat uptake. Their analysis also revealed that the ocean heat uptake efficiency varies by a
48 factor of 2 across the models.

49 To make further progress with identifying the sources of the model spread and model
50 biases revealed by these intercomparisons, more detailed, i.e. process-based analyses are re-
51 quired, employing the individual terms in the temperature tendency equation like advection,
52 the different kinds of diffusion, convection, or ice physics.

53 1.1 Definitions

54 Before we proceed to a discussion of the previous work in this field we need to clearly
55 define the terms we will use. We find that in the literature there is some ambiguity about
56 which OHU processes are called “advective” and “diffusive”. This warrants clarification.
57 There are different ways to define these two terms. In the real ocean, almost all processes
58 that distribute heat are advective, from large-scale currents and mesoscale eddies through to
59 local small-scale turbulence. In this view, the only properly diffusive process is molecular
60 diffusion. In a given ocean model however, the OHU processes fall first of all into two
61 categories, “resolved” and “unresolved”. A subset of the unresolved processes is covered by
62 parameterizations; these processes are thus often called “parameterized”. Obviously, these
63 categories are a function of the model’s grid scale. Processes that are resolved in model
64 A might be parameterized in model B. There is also a tendency to call, in models, resolved
65 processes “advective” and parameterized processes “diffusive”. This arises because resolved
66 processes are captured by the model’s advection scheme, and because many sub-gridscale
67 processes are parameterized as diffusion.

68 It follows that the labels “advective” and “diffusive” depend on the model’s grid scale.
69 This makes a comparison of models with different grid scale difficult, since these labels are
70 not consistently defined across models. We will discuss an example below: whether we call
71 mesoscale eddy-induced heat transports “advective” or “diffusive” is a matter of interpreta-
72 tion. For another example, a model with a grid scale of 0.1° might not need a parameteriza-
73 tion for isopycnal mixing or eddy-induced mixing because its advection contains all these

74 processes. On the other hand, a model with a grid scale of 1° will have parameterisations
75 for these processes, and its advection contains only the large-scale processes. But even in
76 models with very similar grid scales, the use (or not) of parameterisations may differ.

77 The advective processes can be decomposed. For the temperature change in a high-
78 resolution (say, 0.1°) ocean model due to advection $\nabla \cdot \bar{\mathbf{v}}T$, we use the customary Reynolds
79 decomposition into a mean part and an eddy part: $\nabla \cdot (\bar{\mathbf{v}}T) = \nabla \cdot (\bar{\mathbf{v}}\bar{T}) + \nabla \cdot \bar{\mathbf{v}}'T'$. Herein,
80 \mathbf{v} is the three-dimensional resolved velocity, T is the temperature, the overbar denotes a
81 temporal average and the prime the deviation from this average. The Reynolds eddy part
82 actually contains any kind of transient variability. The sum of the temperature change due
83 to the mean advection and the temperature change due to the eddy advection is called here
84 the temperature change due to the *residual* advection. The residual advection is equivalent
85 to the resolved advection in high-resolution models.

86 In the literature, this decomposition of the advective temperature change is used with
87 ocean models that are eddy-permitting or high-resolution (e.g. Wolfe et al, 2008; Morrison
88 et al, 2013, and this study), where “eddy” now rather refers to mesoscale eddies. If ocean
89 models with a coarser resolution are analysed (typically 1° or larger), then this decompo-
90 sition is not made and $\nabla \cdot \bar{\mathbf{v}}T$ change is simply called “advective” (Brierley et al, 2010) or
91 “resolved advective heat flux” (Hieronymus and Nycander, 2013).

92 In coarser resolution models, usually a parameterization of the eddy advective heat trans-
93 port is used, based on Gent and McWilliams (1990). This temperature change due to param-
94 eterized eddy advection is often called “GM flux” (Brierley et al, 2010). It should not be
95 confused with the temperature change due to resolved eddy advection, as defined above.

96 In coarser resolution models as well as in some eddy-permitting models (resolution of
97 $1/3^\circ$ or $1/4^\circ$), often a parameterization of isopycnal mixing is used, too. Examples of eddy-
98 permitting models using an isopycnal diffusion parameterization are this study and NEMO
99 in the $1/4^\circ$ configuration used for the UK Met Office climate models (Megann et al, 2014).
100 Examples of eddy-permitting models not using an isopycnal diffusion parameterization are
101 Wolfe et al (2008); Morrison et al (2013) and Griffies et al (2015). In the latter models it
102 is assumed that the resolved advection by the “permitted” eddies leads to sufficient mixing
103 along isopycnals. However, in some eddy-permitting ocean models that are part of coupled
104 AOGCMs (this study and Megann et al, 2014), it is found that the use of an isopycnal mix-
105 ing parameterisation, based on diffusion, is necessary to obtain a realistic stratification in
106 the ocean. The consequence for our discussion here is that, for the models used in Wolfe
107 et al (2008) and Morrison et al (2013), the temperature change due to eddy advection im-
108 plicitly contains the temperature change due to isopycnal mixing, while for the model used
109 in this study (HiGEM1.2) the temperature change due to eddy advection and the tempera-
110 ture change due to parameterized isopycnal mixing are diagnosed separately. This makes a
111 direct comparison less than straightforward. Ideally, in future studies of ocean heat uptake
112 processes in high-resolution models the advective and diffusive components of the resolved
113 eddy-induced transports should be diagnosed separately, using the methods by Lee et al
114 (2007) and Eden and Greatbatch (2009). In this context, “diffusive” means “behaving like
115 diffusion if seen from a large-scale perspective”.

116 Conceptually it is not clear how to separate isopycnal mixing from eddy advection. As
117 Hieronymus and Nycander (2013) point out, isopycnal mixing could be seen as an advective
118 flux like eddy advection. It is just that isopycnal mixing is often parameterized as diffusion,
119 while eddy advection is either resolved or parameterized as advection. This is the main rea-
120 son why these processes are treated differently in many studies. On the other hand, the eddy
121 advection and the mean advection can be added together and called the residual advection,
122 and it is the residual advection that is actually physically relevant for the tracer transport. In

123 other words, while it can be argued that the eddy advection should be added to the isopycnal
124 mixing, the same eddy advection can arguably alternatively be added to the mean advection.

125 To sum up, ocean model studies sometimes use the terms “advective” and “diffusive”
126 arbitrarily. These terms can also depend on the model resolution and/ or the viewpoint of the
127 analysis of the data. This can lead to confusion in model intercomparisons. Eventually the
128 community might want to find a clearer terminology, perhaps by referring to the actual (real
129 ocean) length scales of the processes.

130 1.2 Previous work

131 In this section we discuss the literature on ocean heat uptake processes that is relevant in the
132 context of the present study. The reader might want to refer to Table 1, in which the models
133 mentioned below, and the largest terms of their heat budgets, are briefly characterized.

134 Detailed temperature tendency diagnostics as mentioned above—for temperature change
135 due to advection, the different kinds of diffusion, convection, ice physics, etc.—were used by
136 Gregory (2000) in HadCM2, to analyse vertical heat transports. He found that on a global
137 scale the main balance is between downward advection of warm waters and an upward
138 transport of heat by mixing along isopycnals. This is in opposition to the often assumed
139 advection-diffusion balance with a downward diapycnal heat transport and an upwelling of
140 warm waters (e.g. Munk and Wunsch, 1998).

141 Using the GFDL ocean model, Gnanadesikan et al (2005) confirmed the result by Gre-
142 gory (2000) that, in a control run, the main process transporting heat downwards (on the
143 global average) is advection, while the upward heat transport is due to subgridscale pro-
144 cesses. These subgridscale processes in Gnanadesikan et al (2005) comprise isopycnal mix-
145 ing, diapycnal mixing and parameterized eddy advection. Parameterized eddy advection is
146 responsible for the bulk of the upward heat transport, while the sum of isopycnal and diapy-
147 cnal mixing transport heat downwards. Gnanadesikan et al (2005) also identified convection
148 as an important process for upward heat transport. Wolfe et al (2008) analysed an eddy-
149 resolving and a high-resolution (5.4 km) OGCM (MITgcm and POP), not using a GM type
150 parameterization of eddy-induced transports. In their models, mean advection and vertical
151 diffusion are warming the ocean, while the resolved eddy advection cools it.

152 Hieronymus and Nycander (2013) used the ocean model NEMO to analyse the vertical
153 heat transport with detailed diagnostics in a long control run. In line with the previous work,
154 they found that mean advection warms the ocean, while the parameterized eddy-induced
155 advection cools it. Parameterized diapycnal diffusion also contributes significantly to the
156 downward heat transport. Hieronymus and Nycander (2013) also looked at the regional fea-
157 tures of the isopycnal heat transport and found that it is concentrated in the Southern Ocean
158 and the North Atlantic.

159 Griffies et al (2015) analysed three versions of the GFDL coupled climate model. Em-
160 phasising the role of mesoscale eddies for ocean heat transport, they confirmed that the
161 strongest downward heat transport comes from the mean advection, followed by vertical
162 diffusion. The largest upward heat transport is due to eddy-induced advection (resolved
163 and/or parameterised), followed by mixed layer physics and parameterized sub-mesoscale
164 eddies.

165 The first study to make use of process-based diagnostics was Manabe et al (1990). They
166 identified the important role of the convection in the Southern Ocean for global ocean heat
167 uptake (OHU). In their control run, deep convection in the high Southern latitudes leads to
168 strong heat loss to the atmosphere. In a $2\times\text{CO}_2$ climate, warming and freshening stabilizes

169 the water column, reducing convection and thus reducing heat loss, which is equivalent
170 to OHU. Gregory (2000) also identified the dominant role of the Southern Ocean for the
171 global heat budget. In a 1%CO₂ run with HadCM2, the ocean warms because of reduced
172 convection that leads to reduced heat loss from convection and isopycnal diffusion.

173 While HadCM2 did not have a GM-type parameterization of eddy-induced processes,
174 Huang et al (2003b) analysed ocean heat uptake processes in a coupled model with a GM pa-
175 rameterization. Again in a 1%CO₂ run, but focusing on an idealized Atlantic, they found that
176 convection, parameterized eddy advection and isopycnal diffusion dominate strong OHU in
177 the high latitudes, and that vertical advection is the dominant process for weaker ocean heat
178 uptake in the lower latitudes. These results are in line with the results from Gregory (2000).
179 However, Huang et al (2003b) have only a single diagnostic for the sum of isopycnal diffu-
180 sion and parameterized eddy advection.

181 Huang et al (2003a) used an OGCM and its adjoint instead of process-based diagnostics
182 to calculate the sensitivities of ocean heat uptake processes to changes in the surface heat
183 flux. In a 1%CO₂ run, they found (similarly to Gregory (2000)) that deep ocean heat uptake
184 happens mostly in the Southern Ocean and in the North Atlantic, due to suppression of
185 isopycnal cooling and of convective cooling. Banks and Gregory (2006) identified reduced
186 surface heat loss and increased precipitation at high latitudes as the causes for an increased
187 stability of the ocean and for the suppression of convection and upward isopycnal diffusion.

188 Brierley et al (2010) analysed the ocean heat budget and heat uptake in HadCM3 using
189 almost the same temperature tendency diagnostics that we will use. Globally, the downward
190 (warming) heat transport in the control run is mainly from resolved advection (downwelling)
191 and to a lesser extent from vertical diffusion. The upward (cooling) heat transport is achieved
192 by parameterized eddy advection (GM) and isopycnal mixing, in accordance with earlier
193 results. In their 1%CO₂ run, the heat uptake is mostly due to isopycnal mixing and, in
194 deeper layers, diapycnal mixing.

195 With a very idealized model, but not using process-based diagnostics, Morrison et al
196 (2013) focused on the roles of the mean and the eddy advection. As in other studies, the
197 mean advection warms the ocean and the (resolved) eddy advection cools it. The residual
198 advection is not analysed. In idealized warming runs, Morrison et al (2013) find (again, in
199 accordance with Gregory (2000)) reduced along-isopycnal mixing (resolved in their model)
200 as the reason for warming. In an increased wind stress run, they find a transient cooling in
201 the ocean interior due to intensified eddy advection in the Southern Ocean.

202 1.3 Aims of the present study

203 The focus, and at the same time the novel aspect, of the present study is to analyse in which
204 regions ocean heat uptake is strongest, and what physical processes dominate it in those
205 regions, in an AOGCM with realistic geography and an eddy-permitting ocean component
206 (HiGEM1.2; Shaffrey et al (2009)), including a detailed set of temperature (and salinity)
207 tendency diagnostics. With HiGEM1.2 being a CMIP5-type model, this analysis also con-
208 tributes to understanding the spread and the biases of projections of thermosteric sea level
209 rise in this class of models.

210 To analyse the causes for changes in ocean heat uptake we conducted two perturbation
211 runs with HiGEM1.2, one run with a scenario of abrupt CO₂ increase and another run where
212 only the windstress was perturbed. The wind perturbation shows the typical southward shift
213 and intensification of the westerlies in the Southern Hemisphere of model scenarios with
214 increased CO₂. The role of the southward shift of the maximum zonal windstress for ocean

215 heat uptake in the 20th century was discussed by Cai et al (2010) for the CMIP3 models.
216 They point out the non-local nature of the ocean heat uptake in the mid-latitude Southern
217 Ocean, and the role of increased Ekman transports.

218 The ocean heat uptake processes we discuss affect the density field in the Southern
219 Ocean, and thus also the flow field, of which the Antarctic Circumpolar Current (ACC) is
220 one of the main features. Wang et al (2011) and Downes and Hogg (2013) discuss the strong
221 role of buoyancy fluxes in determining the response of the ACC in a given GCM to changes
222 in radiative forcing. We will show how the buoyancy fluxes determine the ACC response in
223 HiGEM1.2, and how this relates to the ocean heat uptake processes.

224 The description of the model, the model runs and the diagnostics are found in sec. 2.
225 The analysis of the ocean heat uptake processes using the temperature tendency diagnostics
226 for the global ocean follows in sec. 3. We then present the regional analysis, with a focus on
227 the Southern Ocean, in sec. 4. The impact of the OHU changes on the ACC are discussed in
228 sec. 5, and the conclusions from the paper's results are drawn in sec. 6.

229 **2 Model and Experiments**

230 HiGEM1.2 is based on the UK MetOffice coupled AOGCM HadGEM1, but has a higher
231 spatial resolution, of 0.83° lat x 1.25° lon (N144) in the atmosphere and $1/3^\circ$ x $1/3^\circ$ with 40
232 levels in the ocean. With its high resolution HiGEM1.2 is comparatively expensive to run. In
233 the ocean, the resolution is considered to be eddy-permitting. Therefore it was chosen to not
234 use a parameterization of eddy-induced advection. This choice improved the representation
235 of sharp tracer gradients (Shaffrey et al, 2009). The lateral mixing of tracers uses the isopyc-
236 nal formulation of Griffies et al (1998) with a constant isopycnal diffusivity of $500 \text{ m}^2/\text{s}$.
237 A biharmonic Gent and McWilliams scheme (Roberts and Marshall, 1998) is employed to
238 reduce noise. For the vertical diffusivity a background profile K_{bg} is prescribed as a linear
239 function of depth, and an expression for vertical diffusivity K_{Ri} as a function of the Richard-
240 son number (following Peters et al, 1995) is evaluated. At every time step and grid box, the
241 larger of K_{bg} and K_{Ri} is applied in the vertical diffusion scheme. Mixed-layer processes are
242 parameterized by the Kraus-Turner scheme, which does most of the vertical mixing. Convec-
243 tion is parameterized as complete mixing according to Rahmstorf (1993). Present-day
244 boundary conditions were chosen for the control run. In particular, the atmospheric CO_2
245 concentration was set to 345 ppmv, reflecting conditions in the 1980s.

246 HiGEM1.2 compares well with observations and other GCMs, as Shaffrey et al (2009)
247 have shown in their detailed description of it. As an example, Fig. 1 displays the globally
248 averaged density profile of HiGEM (green) which is close to observations (black) at most
249 depth levels. In line with most CMIP5 models, HiGEM shows open-ocean deep convection
250 in the Southern Ocean, namely in the Weddell and Ross gyres (Heuzé et al, 2013). This
251 process itself is not realistic, yet it leads to realistic water mass properties in the Southern
252 Ocean. HiGEM compares favourably with most CMIP5 models in this regard (Heuzé et al,
253 2013). The presence of open-ocean convection goes along with a sea ice cover (mainly the
254 sea ice fraction) that is less than observations in the control run.

2.1 Perturbation runs

The control run (“CTRL”) length is 111 years upon the beginning of the two perturbation runs, which are labeled 4xCO₂ and WIND. These two runs are only twenty years long because of the computationally expensive resolution of HiGEM.

For the 4xCO₂ run, the atmospheric CO₂ content was quadrupled instantaneously to 1380 ppmv. While this is an idealized scenario, it is one of the standard CMIP5 scenarios (although our run is shorter). In particular, Good et al (2011, 2012) showed that the results of a 4xCO₂ run can be scaled to emulate the results from a 1%CO₂ run with only small errors, especially for temperature.

For the wind perturbation run (“WIND”), we diagnosed the monthly mean wind stress fields from the years 11-20 of the 4xCO₂ run, subtracted the same field from the control run and thus calculated a mean seasonal cycle of the wind stress response. Since we are interested in the effect of wind forcing on the Southern Ocean, these response fields were set to zero north of 10° S and linearly tapered to zero in the latitude band between 20° S and 10° S, where the zonal average of the anomalies is close to zero anyway. In the WIND run, the windstress applied to the ocean is the sum of the windstress computed during the run and the prescribed perturbation as function of the time of year. The wind stress perturbation affects only the momentum flux into the ocean, not the bulk formulae for the tracer fluxes.

Fig. 2 shows the zonal wind stress of the control run and the annual mean tapered anomalies. As in many CMIP5 models, the anomalies reflect a poleward shift and a strengthening of the westerlies in the Southern Hemisphere. Equatorwards of the mid-latitude wind stress maximum the meridional gradient of the wind stress intensifies. While this wind stress perturbation is derived from a 4xCO₂ run, a similar wind perturbation would result from a stratospheric ozone depletion (Sigmond et al, 2011).

2.2 Diagnostics of OHU processes

HiGEM has been run with diagnostics for the individual terms of the temperature and salinity equations. These terms, listed in Table 2, comprise the temperature and salinity change due to diffusion (separately in the x, y and z directions), advection, convection, mixed layer physics, ice physics, penetrating solar radiation (for temperature only) and other surface fluxes. In the absence of a GM-type parameterisation, the advection diagnostic naturally contains the (permitted) eddy activity, and therefore represents the effect of the residual advection. (The effect of the biharmonic GM scheme is included in the three diffusion diagnostics.) At each time step the full three-dimensional fields of these terms are diagnosed, and the monthly (and longer-term) means are saved. The original units of the temperature diagnostics are K/s. By multiplying them with the specific heat capacity C_p and a reference density ρ_0 and averaging them over each model layer individually (or over other volumes, as described below) we obtain the unit of W/m³. In this way, the depth profile figures (starting with Fig. 3) show the change in heat content due to each individual process in each layer. The units suggest interpreting the diagnostics as heat convergences. This is found to be more revealing than the vertical integral of this quantity, in the units of a heat flux, since the convergences describe each layer individually.

We have calculated the temporal standard deviation of the individual diagnostics and their sum with the aim of assessing the significance of the anomalies in the perturbation runs. The section of the control run that we analysed is 70 years long, while the perturbation runs are parallel to the first 20 years of the control run section. We calculate a standard deviation

300 from seven consecutive 10-year means of the control run. A 20-year mean anomaly from
 301 the perturbation run on a given level is considered significant if it is outside the 5% to 95%
 302 confidence interval (1.65σ) interval around the control run value, and there is an additional
 303 factor of $1/\sqrt{2}$ to account for the comparison of a 20-year mean with 10-year means.

304 2.3 Decomposition of diagnostics

305 The run-time diagnostics available for HiGEM are a complete set in that their sum gives the
 306 total temperature change at any gridpoint. However, they do not resolve all the processes
 307 that are relevant. Specifically, this applies to vertical diffusion and advection. The runtime
 308 diagnostic for vertical diffusion is the sum of four processes: (1) the vertical component of
 309 isopycnal diffusion, (2) the background diapycnal diffusion or the shear-dependent vertical
 310 diffusion, (3) vertical diffusion in the mixed layer (following Large et al (1994)) and (4)
 311 the vertical component of the biharmonic GM scheme. The shear-dependent mixing and the
 312 vertical diffusion in the mixed layer only affect the top 100 m or so and we do not discuss
 313 them further, but it is of great interest to decompose the vertical diffusion into its isopycnal
 314 and diapycnal component. Introducing them as further runtime diagnostics would have been
 315 desirable, but is difficult due to the way vertical diffusion is handled in the HiGEM code.
 316 The biharmonic GM scheme is believed to make very small contributions to heat transport
 317 on the large scale; we do however not have a separate online diagnostic for it for the same
 318 reason.

319 We use the Partial Ocean Tracer Tendency Emulator (POTTE) to decompose the vertical
 320 diffusion diagnostic. POTTE is a set of IDL scripts that allows to infer the fields of some of
 321 the tendency diagnostics from the standard output fields temperature, salinity and velocity.
 322 It was modeled on the numerical schemes of the AOGCM HadCM3. POTTE can currently
 323 emulate the fields of temperature change due to advection, isopycnal diffusion (by spatial
 324 components), diapycnal diffusion and advection due to the Gent-McWilliams parameteriza-
 325 tion of eddy-induced transports. In principle, POTTE can thus provide these diagnostics for
 326 any AOGCM or OGCM where only standard output is available. A more detailed description
 327 of POTTE is given in Exarchou et al (2015).

328 By construction POTTE works well for HadCM3. We have tested it for advection and
 329 isopycnal and diapycnal diffusion with HiGEM and found that it works well, too, for advec-
 330 tion and isopycnal diffusion. For diapycnal diffusion however, we found a marked negative
 331 bias in POTTE. Therefore we use POTTE to calculate the temperature change due to the
 332 vertical component of isopycnal diffusion. The difference between the runtime diagnostic
 333 for vertical diffusion and this POTTE result is then interpreted as the temperature change
 334 due to diapycnal diffusion.

335 In addition to the decomposition of vertical diffusion, it is also desirable to decompose
 336 the advection. Since there is no parameterization of mesoscale eddy-induced transports in
 337 HiGEM, the advection diagnostic represents the action of the residual advection in the tem-
 338 perature equation. But it is important to know what part of the temperature change is due to
 339 the mean advection, and what part due to the eddy advection. Following the decomposition
 340 given in sec. 1.1, we use POTTE to calculate the advective temperature change from annual
 341 means and interpret this as the mean advective change $\nabla \cdot (\bar{\mathbf{v}}\bar{T})$. The difference between the
 342 residual advection and the mean advection is then interpreted as the eddy advective temper-
 343 ature change $\nabla \cdot \overline{\mathbf{v}'T'}$.

344 3 Global ocean heat uptake processes and their changes

345 3.1 Global average of the control run

346 In this section we discuss the globally averaged OHU diagnostics and compare them with
 347 other models. A comparison with observational data is highly desirable, but currently not
 348 feasible due to lack of a global coverage of process-based observations. OHU is defined as
 349 a change in ocean heat content (OHC), where for a given volume V : $OHC = \int_V C_p \rho_0 \theta dV$.
 350 Herein, C_p is the specific heat capacity of sea water, ρ_0 a reference density, and θ the po-
 351 tential temperature. (For the calculations, we used a constant value of $\rho_0 C_p = 4.09169 \cdot$
 352 $10^6 \text{ J m}^{-3} \text{ K}^{-1}$.)

353 The global integral of all the diagnosed processes vanishes, except for the two compo-
 354 nents of the surface fluxes that are diagnosed (see Table 2) and an issue with the advection
 355 (see sec. 4.5 for details). The incoming penetrating solar (shortwave) radiation warms the
 356 ocean, and the other (i.e. longwave) surface fluxes cool it. The sum of these two compo-
 357 nents is very small, as we will discuss later. The net warming of the 4xCO2 run is due to
 358 less cooling.

359 The vertical structure of the diagnostics, in the control run and the anomalies, is shown
 360 in Fig. 3. For this and the following figures, we use a power law scaling for both axes,
 361 reflecting the closer spacing of model levels in the upper ocean, and the fact that the diag-
 362 nostics vary across several orders of magnitude. In the literature, a logarithmic scaling of the
 363 axes is often used for such greatly varying variables. This was not applicable here since the
 364 diagnostics may have values of either sign or may even equal zero. Hence we have scaled
 365 the axes with an exponent of 0.3. Because of this scaling, terms which appear to have fairly
 366 modest differences may actually differ by a substantial ratio. To help the reader, the vertical
 367 thin dotted lines indicate orders of magnitude. We use this method of presentation so that
 368 we can accommodate the whole ocean on a common x-axis and thus facilitate comparison
 369 between different depth levels in the same panel. As opposed to the presentation of similar
 370 quantities in the literature (e.g. Hieronymus and Nycander (2013)) using linear scales and
 371 multiple panels, with our method all the terms can be readily identified and compared at
 372 each individual level.

373 Fig. 3a shows profiles of the diagnostics from the 70 years of control run in thick lines.
 374 Thin lines indicate ± 1 standard deviation calculated from seven 10-year means. The upper
 375 100 m are not discussed because the diagnostics are very noisy there, and we are interested
 376 in the processes with longer time scales in the deeper ocean. For the sake of clarity we only
 377 plot the most relevant diagnostics in Fig. 3. The convection diagnostic, and the sum of the
 378 convection diagnostic and the mixed layer physics diagnostic, labelled “VM” for “vertical
 379 mixing”, are plotted separately. The other diagnostics (cf. Table 2) are either very small or
 380 affect only the surface layers.

381 From Fig. 3a we see that in the control run of HiGEM1.2 different processes dominate at
 382 different depth levels. In the global horizontal average we only see the vertical component of
 383 the processes. From below 300 m down to about 3000 m the ocean is warmed by the residual
 384 advection (purple curve) and to a lesser extent by diapycnal diffusion (blue). The warming
 385 due to residual advection can be decomposed (Fig. 3b): the heating is due to the mean
 386 advection (yellow curve), while the eddy advection (dark green) is cooling the ocean. The
 387 flattening of the isopycnals associated with eddy advection redistributes the water masses
 388 such that, on average, warmer waters are displaced upwards, and colder waters downwards.

389 The warming by the residual advection is largely balanced by isopycnal diffusion (Fig. 3a,
 390 green) below 300 m, and to a lesser extent by vertical mixing (orange). At these depths, ver-

391 tical mixing is dominated by convection (dotted orange). In short, for depths between 250 m
392 and 3000 m, the main balance for the heat budget of the ocean is between advective warming
393 and isopycnal cooling. HiGEM1.2 is similar to other AOGCMs in this regard, like Gregory
394 (2000) and the model intercomparison by Exarchou et al (2015), of which HiGEM1.2 is
395 part.

396 The cooling through eddy advection is seen in other eddy-permitting models, e.g. CM2.5
397 and CM2.6 in Griffies et al (2015), or the idealized model used in Morrison et al (2013).
398 Fig. 1 in Morrison et al (2013) seems to indicate that their residual advection is cooling the
399 ocean, in contrast to our results. In the absence of parameterisations for isopycnal diffusion
400 and for eddy advection, their temperature change due to eddy advection (red curves) contains
401 both these processes. This might be the reason for the cooling dominating. As Fig. 3b shows
402 for our model, the cooling due to isopycnal diffusion and due to eddy advection are of
403 comparable magnitude. Indeed, if we added the isopycnal diagnostic (green) to the residual
404 advection diagnostic (purple), the resulting “super-residual” would be close to zero between
405 300 m and 3000 m (not shown).

406 In contrast to Morrison et al (2013), Brierley et al (2010) use an AOGCM (HadCM3)
407 with parameterizations for both isopycnal diffusion and eddy advection. Still, similar to our
408 model, resolved advection and, to a lesser extent, diapycnal diffusion are warming the ocean,
409 while parameterized eddy advection and isopycnal diffusion are cooling it. These results are
410 confirmed for the AOGCMs in Exarchou et al (2015).

411 Below about 3500 m the balance of processes is different. Here, diapycnal diffusion
412 (blue in Fig. 3a) warms the waters while residual advection and convection cool it. This
413 could be explained by cold Antarctic Bottom Water (AABW) being advected from the
414 Southern Ocean and warming by diffusion from the warmer North Atlantic Deep Water
415 (NADW) above. However, the individual processes are not in equilibrium in HiGEM, as
416 their sum, the total (black) is not zero. This non-zero total mirrors the drift in the HiGEM
417 control run. Nevertheless, the total is at least half an order of magnitude smaller than the
418 dominant processes at almost all levels, and one order of magnitude smaller above 700 m.
419 Note that HiGEM1.2 does not have a parameterization of geothermal heat flux, which can
420 be an important part of the heat budget in the abyss (Hieronymus and Nycander, 2013).

421 Fig. 3a also shows the standard deviations of the individual diagnostics (thin lines, 1σ
422 intervals). For most diagnostics and at most depth levels, they are so small that they are not
423 visible in the figures. For the total, the 1σ interval straddles the zero line between about
424 3000 m and 4000 m depth, and above 600 m. This means that the drift is not significantly
425 different from zero in those levels. By contrast, the individual diagnostics are significantly
426 different from zero virtually everywhere.

427 The balance of OHU processes in HiGEM is rather similar to the widely used OGCM
428 NEMO, as a comparison of our results with those of Hieronymus and Nycander (2013)
429 shows. They analysed a long integration of NEMO 3.2 with a 1° resolution. Like in HiGEM,
430 this is a present-day control run. Their “heat trends” (their Fig. 2) differ from our diagnostics
431 only by a factor of the total surface of each ocean layer. In this NEMO run, residual advection
432 warms the ocean between 600 m and 2500 m, and cools it below. However, at most depth
433 levels the warming from vertical diffusion is stronger than from residual advection. This
434 is unusual for a model with realistic topography. The advective warming is balanced by
435 isopycnal diffusion. This is again a typical feature. Below 3000 m there is a balance between
436 advective cooling and warming from diapycnal diffusion, again much as is HiGEM.

437 Wolfe et al (2008) analyzed the global vertical heat flux in two models, MITgcm and
438 POP. Comparing POP (having a realistic topography) with HiGEM1.2 (Fig. 3a), we see
439 again some similarities. In both models, mean advection warms the ocean down to a level

440 between 3500 m (POP) and 4000 m (HiGEM1.2). By contrast, eddy advection cools the
441 ocean down to a level around 3500 m. Both in POP and in HiGEM1.2, the mean and the eddy
442 advection swap signs below that depth. This can be attributed to the northward advection of
443 cold AABW, as in Hieronymus and Nycander (2013). For the next largest term, diapycnal
444 diffusion, there are differences. In HiGEM, the warming effect of vertical diffusion is very
445 small, or even negative, between 1500 m and 3000 m. In POP, vertical diffusion warms
446 the ocean everywhere above 4500 m. As opposed to POP, HiGEM1.2 has also significant
447 convective cooling beyond the winter mixed layer depth, i.e. down to a level of about 2000 m
448 (see further discussion in sec. 4.4).

449 Overall, we conclude that HiGEM1.2 is a typical AOGCM in terms of its ocean heat up-
450 take processes, with warming from residual advection and isopycnal cooling being the most
451 important processes on the global average. Comparison with other models reveals many
452 differences in detail of the relative importance of the processes.

453 3.2 Global changes

454 How does the balance of heat transport processes change in the 4xCO₂ and WIND runs? To
455 address this question we compare the anomalies, which we define as the 20-year averages
456 of the perturbation runs minus the 20-year average of the same period of the control run.
457 We assume that in this way the impact of the residual drift is eliminated. The 4xCO₂ signal
458 of warming (black in Fig. 3c) is bigger than the drift in CTRL (black in Fig. 3a), but it is
459 noteworthy that between 800 m and 2000 m depth they are of the same order of magnitude.
460 This similarity of size is undesirable, and is known to result from insufficient length of
461 spinup runs and imperfect parameterizations of subgridscale heat transport processes. Sen
462 Gupta et al (2012) assessed the ratio of model drift to the 20th century ocean warming.
463 Compared with their results, HiGEM1.2 with its drift to trend ratio of roughly 50% at depth
464 is in line with its parent model HadGEM1 and indeed with all CMIP3 models analyzed in
465 Sen Gupta et al (2012).

466 The total heat content increases by 950 ZJ (1 ZJ = 10^{21} J) in the 4xCO₂ run, equiva-
467 lent to a heat flux of 4.1 W/m² through the ocean surface. The depth structure of the 4xCO₂
468 anomalies is shown in Fig. 3c (note the different scale on the x-axis). There is warming at all
469 depth levels down to the bottom (black curve), even though we analyse only the first twenty
470 years. In the top 1000 m, the warming comes mainly from the vertical mixing processes
471 (orange curve in Fig. 3c). Comparison with Fig. 3a reveals that this warming is actually a
472 reduction of cooling. This, in turn, is connected with a general reduction of mixed layer
473 depth, leading to a reduction in warming due to mixed layer physics (mainly above 500 m,
474 where convection, dotted orange, is small) and convection (below that). Below 1000 m, the
475 ocean is warmed mainly by increased downwelling. There is a small contribution to the
476 warming from reduced isopycnal cooling (compare the green curves in Fig. 3c and Fig. 3a).
477 This could be explained by the vertical structure of the warming, which is stronger at the sur-
478 face than at depth. As a consequence, the along-isopycnal temperature gradient is reduced,
479 leading to reduced isopycnal cooling.

480 It is also noteworthy that there is a substantial reduction of diapycnal warming in Fig. 3c.
481 The reason for this is not immediately obvious since the increased vertical temperature gra-
482 dient should lead to stronger diapycnal warming. Further analysis (not shown) reveals that
483 the decreased diapycnal warming is located in the mid- to high latitudes of both hemispheres.
484 Possibly, our offline calculations of isopycnal diffusion (cf. sec. 2.3) overestimate the reduc-
485 tion of isopycnal cooling in these regions in the presence of the strong isopycnal tilt. Due

486 to our indirect method of determining diapycnal diffusion (explained in sec. 2.3), this might
487 lead to the apparent reduction of diapycnal warming seen in Fig. 3c.

488 We have tested the anomalies of the perturbation run for significance, as explained in
489 sec. 2.2. A non-significant anomaly at any level is marked by an “x” in Fig. 3c and Fig. 3d.
490 Given the small standard deviations in the control run, most of the anomalies are actually
491 significant.

492 The WIND run (Fig. 3d) mainly redistributes heat, and there is only a small net global
493 warming of the ocean of 39 ZJ, or 0.17 W/m^2 . This is remarkable since it could have been
494 expected that the surface fluxes are modified as a result of the effect of the wind stress forc-
495 ing. The anomaly of the total (black curve) is dominated by changes in the downwelling
496 (purple) as the close proximity of these two curves reveals. The anomaly is significant be-
497 tween 700 m and 3000 m. To some extent, the warming trend between 700 m and 1700 m
498 is counteracted by increased cooling from vertical mixing (orange), i.e. convection. Thus,
499 convection has effects of opposite sign in the two perturbation runs. The reasons for this will
500 be explored in sec 4.4.

501 Reduced vertical mixing, from convection and mixed layer physics, and increased down-
502 welling are the main warming processes in idealized CO_2 runs in other models, like HadCM3
503 and MPI-OM (Exarchou et al, 2015). Note, however, that there can be a time dependence.
504 While this study considers the first 20 years of a $4\times\text{CO}_2$ run, Brierley et al (2010) anal-
505 yse a $1\%\text{CO}_2$ run from HadCM3 after 70 years. In that run, they find that vertical mixing
506 and isopycnal mixing are the dominant warming processes, while advection plays a lesser
507 role. Similarly, in the MITgcm, Huang et al (2003a) found that reduced vertical mixing and
508 reduced isopycnal cooling are the most important processes leading to warming (although
509 their ocean model is forced by relaxation, as opposed to the AOGCMs with heat conserva-
510 tion).

511 Whether there is a net warming in a WIND-type run seems to depend on details of
512 the applied forcing. Frankcombe et al (2013) found that their eddy-permitting ocean model
513 warms for a merely increased wind speed, while for a poleward shift in the wind speed
514 maximum their ocean cools, in contrast to the present study. Note that Frankcombe et al
515 (2013) modified wind speed, not wind stress. Thus, in their case the surface buoyancy fluxes
516 are affected by the wind forcing too, which might well influence the ocean’s heat budget. The
517 eddy-permitting model by Morrison et al (2013) shows a net warming, too, for an increased
518 wind stress.

519 **4 Regional ocean heat uptake processes**

520 We analyse now the regional differences between $4\times\text{CO}_2$ and WIND in terms of ocean heat
521 uptake, with the aim of understanding where the changes discussed in the previous section
522 actually happen. The global ocean heat uptake pattern (Fig. 4) is defined as the difference
523 in the ocean heat content, averaged over 20 years, between the perturbation runs and the
524 control run, expressed as the vertical column integral in GJ/m^2 . Fig. 4 shows that in the
525 Southern Ocean there is a band of large OHU in the mid-latitudes (around 40° S to 50° S)
526 in both runs. The $4\times\text{CO}_2$ run (Fig. 4a) shows regions with large heat uptake in the North
527 Atlantic, in the Arctic and to a lesser extent in the North Pacific. With the exception of some
528 small signal in the North Atlantic, this OHU in the Northern Hemisphere does not happen
529 in the WIND run (Fig. 4b). From comparing Figs. 4a) and b) we can infer that the OHU
530 maxima in the mid-latitude Southern Ocean are mainly wind-driven, since they appear in
531 both the perturbation runs. By contrast, we expect the ocean heat uptake in the high-latitude

532 Southern Ocean to be driven by the surface fluxes, since it does not appear in the WIND run.
 533 The regional pattern of OHU in HiGEM is a typical representative of the CMIP5 models,
 534 as a comparison of Fig. 4a) with Kuhlbrodt and Gregory (2012) (their Fig.2, supplement)
 535 reveals.

536 For discussing the regional features, we define a few latitude belts that we will discuss
 537 in turn:

- 538 – Northern Extratropics (“NEx”): 30° N to 90° N
- 539 – Tropics: 30° S to 30° N
- 540 – Southern Hemisphere, mid-latitudes (“SHeMi”): 60° S to 30° S
- 541 – Southern Hemisphere, high latitudes (“SHeHi”): 90° S to 60° S

542 Furthermore, there are some specific regions that we will refer to, which are outlined by
 543 green rectangles in Fig. 4:

- 544 – Southwest Indian Ocean (“In”): 20° E to 75° E and 43° S to 37° S
- 545 – Argentine Basin (“Ar”): 58° W to 0° E and 50° S to 35° S
- 546 – Weddell Gyre (“W”): 55° W to 0° E and 75° S to 62° S
- 547 – Ross Gyre (“R”): 178° W to 138° W and 75° S to 65° S
- 548 – Drake Passage (“DP”): 69.33° W to 68° W and 68° S to 55° S

549 The profiles of the advection diagnostic have to be interpreted differently now since the
 550 volumes over which the advective heating is averaged have lateral boundaries. Thus, as
 551 opposed to the global averages, there will be a lateral advective heat transport, which cannot
 552 be separately diagnosed. The other diagnostics (diapycnal mixing, the vertical component
 553 of isopycnal mixing, convection and mixed layer physics) are vertical by definition, so their
 554 interpretation does not change.

555 4.1 Northern Extratropics

556 In the Northern Extratropics, the heat budget is dominated in the control run by advective
 557 warming down to about 2000 m (purple line in Fig. 5a). This is balanced mostly by vertical
 558 mixing (orange line), which is mostly convection (dotted orange) below ~ 700 m, and to
 559 some extent by isopycnal cooling (green line), especially at depths between 300 m and
 560 700 m. Diapycnal mixing plays a minor role in warming the ocean. Below 2000 m, the
 561 heating/cooling rates are very small. The total warming rate is not significantly different
 562 from zero in the top 1000 m, where the magnitude of the heating/cooling processes is large.
 563 There is a slight positive drift below 1000 m.

564 As is visible in Fig. 4a, the Northern Extratropics warm up significantly in 4xCO₂.
 565 Fig. 5c shows that this is largely due to decreased warming by mixed layer physics since the
 566 total warming (black) is almost fully explained by the positive anomaly of vertical mixing
 567 (orange), with the convection anomaly (dotted orange) small or negative above ~ 700 m.
 568 Reduced isopycnal cooling plays a minor role, and there is some compensating reduced di-
 569 apycnal warming (blue). In WIND there is no significant OHU in the Northern Hemisphere.

570 In the Arctic Ocean proper (not shown) the warming is actually mostly advective, and
 571 reduced convection is less important for the warming. The mixed layer depth is very small
 572 already in the control run, and is further diminished by a strong freshening in the surface
 573 layer (from sea ice melt). This suggests that the warming in the Arctic is due to lateral
 574 advection from the North Atlantic.

575 4.2 Tropics

576 In the Tropics region, the heat budget in the control run is a balance between diapycnal
577 downward heat flux (blue line in Fig. 5b) and an upward and/or lateral advective heat trans-
578 port (purple) in the top 1000 m. Thus, we find here the classical advection-diffusion bal-
579 ance (e.g. Munk and Wunsch, 1998). Contrary to their assumption, neither is this balance
580 found in other regions of the world ocean, nor is the global heat budget dominated by the
581 advection-diffusion balance. Rather, the global budget is dominated by downward advective
582 heat transport and upward isopycnal diffusion of heat (Fig. 3a). Our results, obtained
583 from a fully coupled AOGCM, confirm earlier results from an idealized ocean-only model
584 (Morrison et al, 2013).

585 In the 4xCO₂ run (Fig. 5d), we find a significant warming between 200 m and 500 m
586 depth, caused advectively, i.e. either by a reduced upwelling of cold waters or by lateral
587 advection. By contrast, in WIND there is an advective cooling, in the same depth range.

588 4.3 Southern Hemisphere mid-latitudes

589 In the Southern Hemisphere mid-latitudes, the heat budget is dominated by downwelling
590 and lateral advection of warm waters, and cooling through isopycnal mixing, on a large
591 range of depth levels, from 300 m down to about 3500 m (Fig. 6). Isopycnal mixing is also
592 the prevailing cooling mechanism on the global average (see Fig. 3). The Southern Hemi-
593 sphere mid-latitudes region is of interest because it contains two regions of strong OHU, in
594 the Argentine Basin and the Southwest Indian Ocean. Notably, this strong OHU occurs in
595 both 4xCO₂ and WIND. Fig. 6b and Fig. 6c reveal that the depth structure of the warm-
596 ing is indeed similar. There is a clear signal of warming in the upper 2000 m or so (black
597 lines). From 400 m downwards, this warming is advectively caused (purple), i.e. down-
598 welling and/or lateral advection are enhanced. Above 400 m there is a large contribution
599 from decreased cooling by vertical mixing (orange, mostly mixed layer physics), more so
600 in 4xCO₂. A detailed analysis (not shown) of the two regions with maximal OHU shows
601 that the windstress changes in both 4xCO₂ and WIND lead to stronger wind stress curl and
602 stronger Ekman pumping. Cai et al (2010) diagnose nonlocal warming from surface fluxes
603 south of 50° S, along with the increased Ekman pumping, as the causes for the warming in
604 the Southern Hemisphere mid-latitudes in the CMIP3 models.

605 4.4 Southern Hemisphere high-latitudes

606 Fig. 7a shows that in the Southern Hemisphere high-latitude region, in the control run, the
607 ocean heat transport processes have a larger magnitude at depth than in the Southern Hemi-
608 sphere mid-latitudes. This is true for advection, but even more so for convection (dotted
609 orange line in Fig. 7a). In this region, convection does nearly all of the vertical mixing be-
610 low ~600 m, as revealed by the close proximity of the dotted orange line (convection) to
611 the solid orange line (convection + mixed layer physics). In the Southern Hemisphere high-
612 latitude region, we find two smaller region of interest, the Ross Gyre and the Weddell Gyre.
613 In these regions the mixed layer is very deep, suggesting ongoing deep-water formation. As
614 Fig. 4 shows, the response in 4xCO₂ and WIND is different here. The deep-water forma-
615 tion regions warm in 4xCO₂, but cool in WIND. Fig. 7b and Fig. 7c show why. In 4xCO₂,
616 in the whole Southern Hemisphere high-latitude region, the warming (black line) reaches

617 much deeper than in the mid-latitudes, and this is due to reduced convection (dotted orange
618 line), whereas in the mid-latitudes, it is advection that is responsible for the warming. In the
619 WIND run, we find a significant cooling at depth (below 1000 m), which is due to increased
620 convective activity. In the eddy-permitting ocean-sea ice model by Frankcombe et al (2013)
621 a similar effect is seen (in their W_{4S} experiment), whereas in the idealized eddy-permitting
622 model by Morrison et al (2013) the mid-depth cooling in the enhanced wind stress exper-
623 iment is attributed to increased eddy-induced cooling. We speculate that the dominance of the
624 heat fluxes due to vertical mixing is a feature of models with realistic topography, explicitly
625 modeled sea ice and a nonlinear equation of state. (In the high-latitude Southern Ocean the
626 dependence of density on temperature is very weak.) In short, in WIND the vertical mixing
627 is decreased in the Southern Hemisphere mid-latitudes—in the depth range 200–500 m rel-
628 evant for that region— but increased in the high latitudes. The heat loss in the high latitudes
629 (and in the tropics) almost compensates the heat gain in the mid-latitudes, such that the net
630 global OHU in WIND is very small.

631 We explore the different response of the deep-water formation sites in 4xCO₂ and WIND
632 in more detail. In 4xCO₂, there is an increase in maximum sea ice cover in the coastal
633 regions, and less sea ice cover away from the coasts (Fig. 8b), while in WIND the sea ice
634 cover decreases almost everywhere (Fig. 8c). (The Ross Gyre is an exception, with increased
635 sea ice cover in both runs.) What we find is that in 4xCO₂ there is a strong freshening in the
636 coastal surface layer, which is not seen in WIND. The source of this freshwater is increased
637 precipitation in 4xCO₂. This freshwater layer increases the vertical density gradient in the
638 surface layer, thus stopping deep water formation. In the WIND run, by contrast, the reduced
639 sea ice cover leads to enhanced deep water formation.

640 The Ross Gyre is a special case because the deep water formation is exceptionally deep
641 there. In the control run, convection is cooling the ocean at almost all levels. In 4xCO₂, the
642 warming is of a similar magnitude at all depth levels down to the bottom (not shown), i.e.
643 as large in the abyss as at mid-depth. The anomalies in 4xCO₂ are thus particularly large.
644 Therefore, the cessation of convection in 4xCO₂ leads to a surface cooling, which does
645 not happen in the other regions in the high-latitude Southern Ocean. It is this cooling that
646 enables the sea-ice cover to expand in the Ross Gyre. Another factor in favour of a build-up
647 of ice cover in the Ross Gyre might be the wind forcing. As Fig. 2b shows, the anomalous
648 wind stress is smaller in the Ross Gyre region than at many other longitudes. We speculate
649 that the weaker wind stress anomaly in the Ross Gyre favours build-up of sea-ice.

650 A similar mechanism of decreased convection was found in a 1%CO₂ run with CCSM3,
651 one of the CMIP3 models (Kirkman IV and Bitz, 2011). They attribute the stabilization of
652 the ocean south of 60° S mainly to a surface freshening, which however comes from a
653 reduction in sea ice growth near Antarctica, a reduced northward sea ice export and more
654 sea-ice melt further south, in contrast to the precipitation changes in HiGEM1.2.

655 4.5 Comparison of the regions

656 A comparative perspective on the ocean heat uptake processes in the regions discussed above
657 is given in Fig. 9. Here, the dominant terms in the entire volume of the individual regions
658 are plotted. The largest terms are advection and the surface fluxes (the two components de-
659 scribed in sec. 3.1 added together). The other diagnostics (e.g. the horizontal components of
660 the diffusion processes) are mostly small; for some regions there is a discernible response
661 in the ice physics, which is however always smaller than the response in the total surface
662 fluxes and the advection. Therefore we have omitted it here, along with the rest of the diag-

663 nostics. Finally, the total sum of the diagnostics is plotted in Fig. 9 (red bars). This contains
 664 all diagnostics, with no omissions. In an integral over the whole water column, as in Fig. 9,
 665 the vertical mixing (VM) and the vertical diffusion diagnostics vanish by construction.

666 For every model run and every region, the magnitude of the three components (surface
 667 fluxes, advection and total heating rate) is plotted in Fig. 9a. In each triplet, the first bar
 668 is for the control run, the second bar is for the 4xCO₂ run (darker hue), and the third bar
 669 is for the WIND run (lighter hue). Fig. 9b shows the anomalies of the perturbation runs.
 670 Therefore there are only two bars in each group: the first bar (darker hue) displays the
 671 4xCO₂ anomaly for each component and region, and the second bar (lighter hue) displays
 672 the WIND anomaly, again for each component and region. For instance, in accordance with
 673 Fig. 4 we see that the Weddell Sea gyre warms in the 4xCO₂ run (larger net heating rate,
 674 dark red bar), but cools in the WIND run (the light red bar indicates a negative heating rate).
 675 By contrast, the mid-latitude Southern Ocean (“SHeMi”) warms in both the 4xCO₂ and the
 676 WIND run, as indicated by the dark red and the light red bar both being positive, while in
 677 the control run there is a net cooling, indicated by the negative first red bar in Fig. 9a.

678 As is to be expected, the high-latitude regions (NEx, SHeHi, Wed and Ros) have a
 679 negative surface heat flux (Fig. 9a), while the mid- and low latitude regions (Tropics and
 680 SHeMi) gain heat from the surface fluxes. The 4xCO₂ warming (the dark red bars) comes
 681 from a reduction of surface cooling in the high-latitude regions (dark blue bars), which is
 682 counteracted by a reduced advective warming (dark green bars). The high-latitude regions
 683 on the Southern Hemisphere are cooling in WIND (negative light red bars), which is mostly
 684 due to a reduced advective warming (light green bars).

685 The Southern Hemisphere mid-latitudes are different, because they are warming in
 686 WIND, and because this warming is due to increased advective warming. By contrast, the
 687 warming in 4xCO₂ in this region is mostly due to increased surface warming, with some sup-
 688 port from advection. This contrast is remarkable because the depth structure of the warming
 689 in these two cases is very similar (Fig. 6).

690 An analysis of the volume-integrated heating rates, as opposed to the volume-averaged
 691 heating rates in Fig. 9, reveals the relative contribution of the individual regions to the global
 692 net warming. These relative contributions are: 26% for NEx, 32% for Trop, 35% for SHeMi,
 693 6% for SHeHi and 1% each for Wed and Ros. In other words, the strongest contribution to
 694 the global net warming comes from the Southern Hemisphere mid- and high latitudes (41%
 695 altogether), followed by the Tropics and eventually the Northern Extratropics.

696 Finally, the global ocean shows a warming from surface fluxes even in the control run—
 697 this is what ultimately causes the drift. There is also a very small advective cooling in all
 698 three runs. This stems from the imperfect way the free-surface boundary condition is for-
 699 mulated in the model; it is not caused by the diagnostics.

700 5 ACC response

701 The Antarctic Circumpolar Current (ACC) is the strongest current in the world ocean. At
 702 Drake Passage, its transport is currently estimated to be 153 ± 5 Sv (Mazloff et al, 2010).
 703 It is intimately linked with the global meridional overturning circulation (MOC). The ACC
 704 and the MOC are the dominant features of the large-scale circulation in the Southern Ocean.
 705 In climate models the strength of the ACC is not well constrained: the model mean from
 706 the CMIP5 models (Meijers et al, 2012) is 155 ± 51 Sv. Thus the ACC strength in Drake
 707 Passage in HiGEM1.2, 190 Sv in CTRL, is within the range of the CMIP5 models.

708 Here we will analyse how the ACC is changing in the perturbation runs, and how this
709 relates to the ocean heat uptake processes. Since the ACC is driven by a combination of
710 wind stress and buoyancy fluxes (Marshall and Radko, 2003), we expect both these forcings
711 to influence the ACC strength. Fig. 10 shows the development of the ACC—measured as the
712 volume transport through the Drake Passage—in the 70 years of CTRL (black line) and in
713 the perturbation runs (red: 4xCO₂, blue: WIND). In the first 20 years of the control run there
714 is a slight downward trend (dashed) of -2.2 ± 0.7 Sv/decade, after which the ACC transport
715 stabilizes around 184 Sv. In 4xCO₂ there is a strong downward trend (-9.1 ± 0.9 Sv/decade),
716 bringing the ACC transport to 175 Sv after 20 years. This weakening of the ACC under a
717 scenario of increased CO₂ forcing is shown by the majority of the CMIP5 models (Meijers
718 et al, 2012).

719 In contrast to 4xCO₂, in WIND the ACC transport strengthens to 200 Sv after 20 years,
720 with an upward trend of 4.7 ± 0.9 Sv/decade. This is remarkable because in other AOGCMs
721 with an eddy-permitting grid resolution in the ocean component (e.g. GFDL CM2.4, Farneti
722 et al, 2010) the ACC strength does not increase under a scenario with increased wind stress.
723 This might seem surprising at first since the nominal resolutions of HiGEM and CM2.4 are
724 similar, namely $1/3^\circ$ and $1/4^\circ$. However, while in HiGEM the grid spacing is constant in
725 latitude and longitude everywhere, in CM2.4 the resolution increases with latitude like in a
726 Mercator grid, such that the actual resolution at 60° S is about $1/8^\circ$. This resolution allows
727 the dynamic response of the eddy field that Farneti et al (2010) describe. By contrast, in the
728 mid- to high-latitudes the resolution of HiGEM only permits a flow field with small-scale
729 standing eddies, but little temporal variability.

730 A reduced ACC transport in climate change simulations has been explained by the nar-
731 rowing of the ACC in combination with processes that affect the baroclinic structure of the
732 ocean and specifically the tilt of the isopycnal surfaces (Wang et al, 2011). We discuss these
733 two causes in turn. The narrowing is defined as a decrease in the area occupied by the ACC.
734 In order to understand the diverging responses of the ACC in the two perturbation runs,
735 we analyse the ACC area, defined as the area between the northernmost and southernmost
736 streamlines that go through Drake Passage, as shown in Fig. 11. In CTRL, this area is about
737 29,200,000 km². In WIND, the ACC area increases by 7%, while in 4xCO₂ it is reduced
738 by 5%. This reduction is mostly due to an enlargement of the subpolar gyre in the Weddell
739 Sea and, in an overlapping longitude range, a poleward shift of the Agulhas Current. The
740 narrowing and weakening of the ACC occurs also in the 2%CO₂ run of HiGEM1.1 (Graham
741 et al, 2012). Here, the DPT is reduced from 176 Sv to 162 Sv, and the narrowing occurs both
742 on the northern flank of the ACC, mainly in the Indian Ocean sector, and on the southern
743 flank, mainly in the regions of the Weddell Gyre and the Bellingshausen Sea. These results
744 are very similar to what we find in HiGEM1.2.

745 To explain why this narrowing occurs we need to understand why the Weddell Gyre is
746 extending. From the barotropic streamfunction (Fig. 11) we see that the the Weddell Gyre
747 is also strengthening, from about 50 Sv in CTRL to 70 Sv in 4xCO₂. The surface density
748 is decreasing in this area, but not in a way that would be particularly strong in comparison
749 with other latitude ranges. Therefore, this cannot explain why the Weddell Gyre expands and
750 strengthens, while the Ross Gyre does not do that. It is more revealing to look at the wind
751 stress changes in more detail. Fig. 2b shows that the wind stress anomalies in the region
752 around 0° E, where the Weddell Gyre spins up, are clearly stronger than in the Ross Gyre
753 region. It is also in this longitude range (between 0° E and 90° E) where the equatorward
754 contraction of the ACC is strongest (Fig. 11).

755 Next we turn to assess the changes in the baroclinic structure. Since these vary consid-
756 erably with latitude and longitude, and since we are interested in the transport through the

757 Drake Passage, we analyse the baroclinic structure and its changes in the Drake Passage
758 region (DP in Fig. 4). As we would expect, the isopycnal surfaces (potential density σ_2)
759 are strongly tilted across DP (colour shading Fig. 12). In line with the changes in DP trans-
760 port depicted in Fig. 10, the isopycnals flatten in 4xCO₂ (Fig. 12a) and steepen in WIND
761 (Fig. 12b). The density changes in 4xCO₂ (denser at the northern end of DP, lighter in the
762 subsurface core section) can be attributed mainly to temperature changes (cooling/warming;
763 not shown). The density changes in WIND—lighter in a wedge-shaped region from the sur-
764 face down to ~ 500 m at the southern end of DP sloping down to ~ 1000 m at the northern
765 end—are, by contrast, mainly caused by freshening. The cooling, in 4xCO₂, at the northern
766 end of DP is mainly caused by a reduction in convection (around ~ 400 m), in mixed layer
767 processes (above that) and in vertical diffusion (below ~ 400 m). The subsurface warming in
768 4xCO₂ comes from the reduced convection, too, but more so from advection, which will be
769 lateral advection in all likelihood, given the presence of the strong current. The freshening
770 in WIND can be largely attributed to advection as well, and to some extent to an increased
771 convective activity. The changes in convective and mixed layer activity in both perturba-
772 tion runs are in accordance with the changes in the mid-latitude Southern Ocean in general
773 (sec. 4.3).

774 We had attributed the different response of vertical mixing in the both perturbation runs
775 to the different freshwater fluxes in sec. 4.4. Thus, we can conclude that the precipitation
776 increase in 4xCO₂ is crucial for explaining both the different response of the ACC and the
777 differences in OHU in 4xCO₂ and WIND. The freshening triggers a reduction of convection
778 in 4xCO₂, leading to net OHU in the full water column, with cooling in the top layer and
779 warming below. These changes in temperature and salinity affect the baroclinic structure in
780 opposite ways in 4xCO₂ and WIND.

781 6 Conclusions

782 The purpose of this paper is to analyse the ocean heat uptake processes globally and region-
783 ally using detailed diagnostics of the temperature tendencies in HiGEM1.2, an AOGCM
784 with realistic geography and an eddy-permitting ocean component. The novelty is the focus
785 on which ocean heat uptake processes are dominating in which regions.

786 For the global heat budget, the Southern Ocean is the most important region, and the
787 dominant balance is between downward advective transport and upward isopycnal diffusion,
788 as found in previous model studies, while in the upper tropical ocean we find the traditionally
789 assumed diapycnal diffusion/upwelling balance. In the Northern Extratropics, convection
790 and mixed layer physics are the most important cooling process, balancing downward ad-
791 vection. The decomposition of the global downwelling shows that the eddy advection cools
792 the ocean, as in several other models. The cooling from eddy advection and from isopycnal
793 diffusion are of the same order of magnitude. It can be argued that they could be added to-
794 gether since they can be both seen as diffusive processes on isopycnals, and combined with
795 mean advection to give a new “super-residual” advection.

796 The advective (that is, due to downwelling and/or lateral advection) warming goes deep-
797 est in the high-latitude regions of the Southern Hemisphere. As a consequence, the changes
798 in the perturbation runs have their deepest extent in this region too. In the Ross Gyre, the
799 warming in 4xCO₂ extends down to the bottom.

800 The 4xCO₂ and WIND runs give quite different results for the high-latitude Southern
801 Ocean area. The ocean heat uptake there in 4xCO₂ is explained by reduced convection,
802 triggered by freshwater input from precipitation. In WIND, there is increased convective

803 activity, and therefore a heat loss from the ocean. Due to the increased precipitation and the
804 ensuing freshwater lid, the same wind stress forcing cannot trigger more convection in the
805 4xCO₂ run.

806 Seen as a whole, the warming in the 4xCO₂ run is due to changes in convection and
807 mixed layer physics in the high latitudes on both hemispheres, and due to advection in
808 the Southern Hemisphere mid-latitudes. In the WIND run, the windstress forcing in the
809 Southern Hemisphere redistributes the heat content, but only leads to a very small global
810 OHU.

811 The interplay of freshwater and wind forcing also explains why the ACC is strength-
812 ening in WIND while it weakens in 4xCO₂. The diminishing ACC in 4xCO₂ is due to a
813 narrowing of the ACC, caused by a wind-driven expansion of the Weddell Gyre, and due
814 to a flattening of the isopycnals caused by the suppression of vertical mixing. Conversely,
815 the enhanced vertical mixing in WIND leads to a steepening of the isopycnals in the Drake
816 Passage and thus to a stronger transport across it.

817 Comparison of our results with other models reveals many differences in detail of the
818 relative importance of the processes. These differences call for a further analysis, in order to
819 relate them to the models' formulation and control states. For this purpose, it would be very
820 helpful to have accurate online diagnostics of all relevant ocean heat uptake processes. This
821 would allow for more accuracy and detail in future model intercomparison studies.

822 A caveat in this study is that the modeled open-ocean deep-water formation in the South-
823 ern Ocean is unrealistic, like in all AOGCMs of a comparable resolution. A similar study in
824 a high-resolution AOGCM would be very interesting if it had a better representation of the
825 on-shelf deep-water formation processes in the Southern Ocean. Still, we believe that such a
826 model would confirm the importance of regional ocean heat uptake processes for the global
827 heat budget and the relevance of salinity changes for some regional changes in ocean heat
828 uptake.

829 **Acknowledgements** We are grateful to Dave Stevens and Ian Stevens for help and support with running
830 HiGEM1.2 and investigating the model code. The comments of Steve Griffies and two anonymous review-
831 ers have led to important clarifications in the paper. The research leading to the results presented here has
832 received funding from the European Research Council under the European Community's Seventh Frame-
833 work Programme (FP7/2007-2013), ERC grant agreement number 247220, project "Seachange", and from
834 the National Centre for Atmospheric Science (NCAS) Climate Programme.

835

Table 1: Overview of the ocean models whose results are discussed in sec. 1.2. The columns, from left to right, give the study we are citing, the horizontal resolution of the ocean model, the number of vertical levels, whether it is a coupled atmosphere-ocean model, whether the GM parameterization has been used, the isopycnal diffusion coefficient (if a parameterization for isopycnal diffusion was used at all), and—in the last column—the largest terms of either sign (warming \oplus or cooling \ominus) of the global heat budget between approximately 200 m and 1500 m depth. Here, the results for the full budget of the control run (**CTL**) are given in upright typeface, and the results for the *anomalous* fluxes in global warming scenarios (CO_2) are given in *italics*. These global warming scenarios are mostly idealized. The abbreviations in the last column are “adv” for resolved advection, “dia” for diapycnal mixing, “iso” for isopycnal mixing, “VM” for vertical mixing (the sum of convection [“conv”] and mixed-layer physics), “mean” for mean advection, “edd” for resolved eddy advection and “GM” for parameterized eddy advection. If two processes are written together with a plus (e.g. “(GM+iso)”) then they have not been diagnosed separately.

Study	Resolution	Le- vels	Coup- led	GM used	Isopyc. diff. coefficient	Largest budget terms glob- ally ($\sim 200 - 1500$ m)
Banks and Gregory 2006	1.25 $^\circ$	20	yes	yes	1000 m ² /s	CO_2 : <i>adv</i> \oplus , <i>VM</i> \oplus
Brierley et al. 2010	1.25 $^\circ$	20	yes	yes	1000 m ² /s	CTL : <i>adv</i> \oplus , <i>GM</i> \ominus CO_2 : <i>iso</i> \oplus , <i>conv</i> \oplus
Gnanadesikan et al. 2005	4.5 $^\circ$ lat \times 3.75 $^\circ$ lon	24	no	yes	1000 m ² /s	CTL : <i>adv</i> \oplus , <i>GM</i> \ominus
Gregory 2000	2.5 $^\circ$ lat \times 3.75 $^\circ$ lon	20	yes	no	400– 2000 m ² /s	CTL : <i>adv</i> \oplus , (<i>iso+dia</i>) \ominus CO_2 : <i>adv</i> \oplus , (<i>iso+dia</i>) \oplus
Griffies et al. 2015: CM2-1deg	1 $^\circ$	50	yes	yes	600 m ² /s	CTL : <i>adv</i> \oplus , <i>GM</i> \ominus
Griffies et al. 2015: CM2.5	0.25 $^\circ$	50	yes	no	none	CTL : <i>mean</i> \oplus , <i>edd</i> \ominus
Griffies et al. 2015: CM2.6	0.1 $^\circ$	50	yes	no	none	CTL : <i>mean</i> \oplus , <i>edd</i> \ominus
Hieronimus and Nycander 2013	1 $^\circ$	46	no	yes	1000 m ² /s	CTL : <i>adv</i> \oplus , <i>GM</i> \ominus
Huang et al. 2003a	4 $^\circ$	15	yes	yes	1000 m ² /s	CO_2 : <i>conv</i> \oplus , (<i>GM+iso</i>) \oplus
Huang et al. 2003b	4 $^\circ$	15	no	yes	1000 m ² /s	CO_2 : <i>conv</i> \oplus , (<i>GM+iso</i>) \oplus (below 700 m)
Manabe et al. 1990	4.5 $^\circ$ lat \times 3.75 $^\circ$ lon	12	yes	no	none	CTL : <i>adv</i> \oplus , <i>conv</i> \ominus CO_2 : <i>conv</i> \oplus , <i>adv</i> \ominus
Morrison et al. 2010	0.25 $^\circ$	36	no	no	none	CTL : <i>mean</i> \oplus , <i>edd</i> \ominus CO_2 : <i>edd</i> \oplus
Wolfe et al. 2008: MITgcm	5.4 km	20	no	no	none	CTL : <i>dia</i> \oplus , <i>edd</i> \ominus
Wolfe et al. 2008: POP	0.1 $^\circ$	40	no	no	none	CTL : <i>mean</i> \oplus , <i>edd</i> \ominus
This study	0.33 $^\circ$	40	yes	no	500 m ² /s	CTL : <i>adv</i> \oplus , <i>iso</i> \ominus CO_2 : <i>VM</i> \oplus , <i>adv</i> \oplus

Table 2: Terms of the tracer transport equations as diagnosed on runtime in HiGEM1.2. Z-diffusion and advection are further decomposed, using POTTE, into the components after the colon.

x-diffusion	ice physics
y-diffusion	mixed layer physics
z-diffusion: isopycnal, diapycnal	convection
penetrating solar radiation	advection: mean, eddy-induced
other surface fluxes	

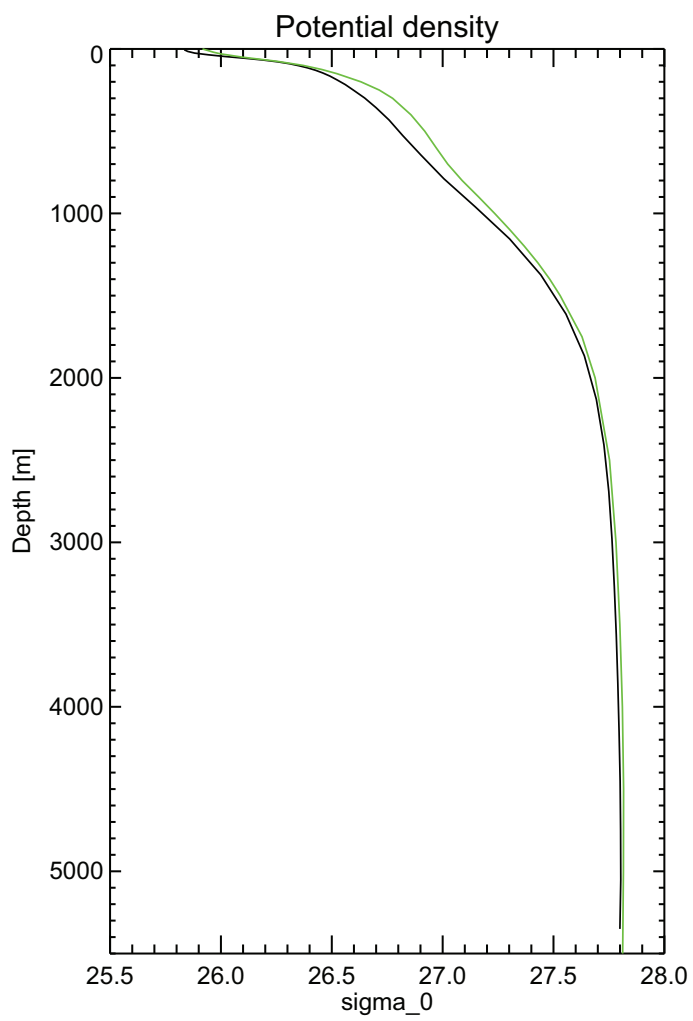


Fig. 1: Globally averaged density profile from the World Ocean Atlas 2009 (black, *Locarnini et al., 2010*) and the HiGEM control run (green, 20-year average).

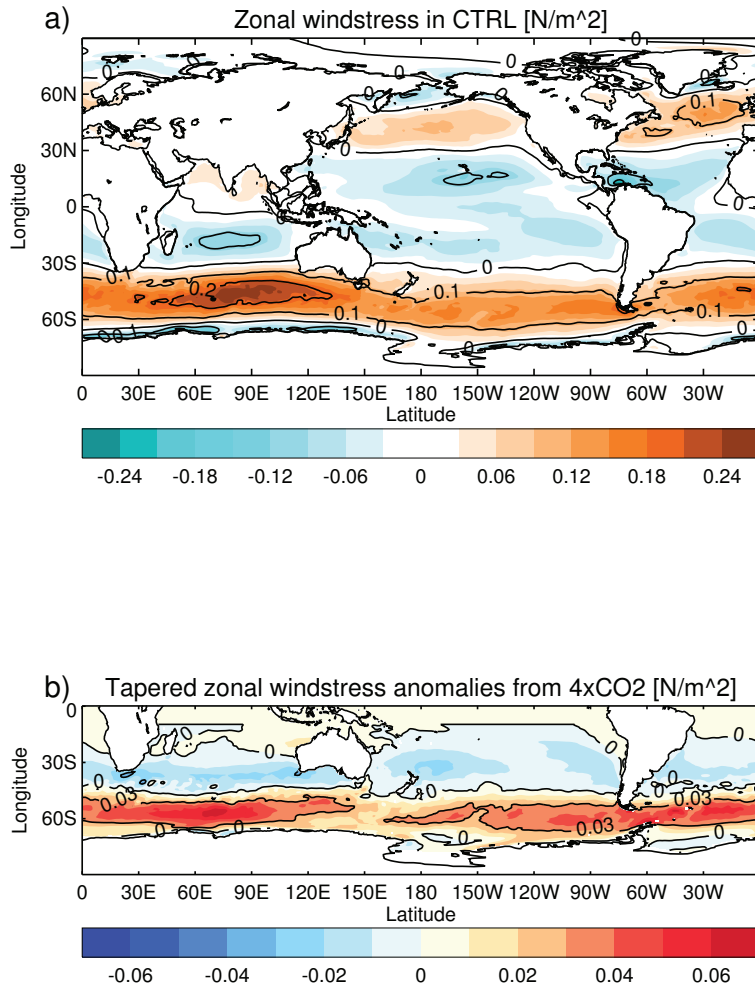


Fig. 2: (a) Zonal windstress in the control run, averaged over model years 2100 to 2110. (b) Anomalies of the zonal wind stress in the Southern Hemisphere in the 4xCO₂ run averaged over the same period and tapered north of 20° S as described in the main text. The intensification of the westerlies is strongest in the Indian Ocean sector and weakest in the southwest Pacific sector of the Southern Ocean.

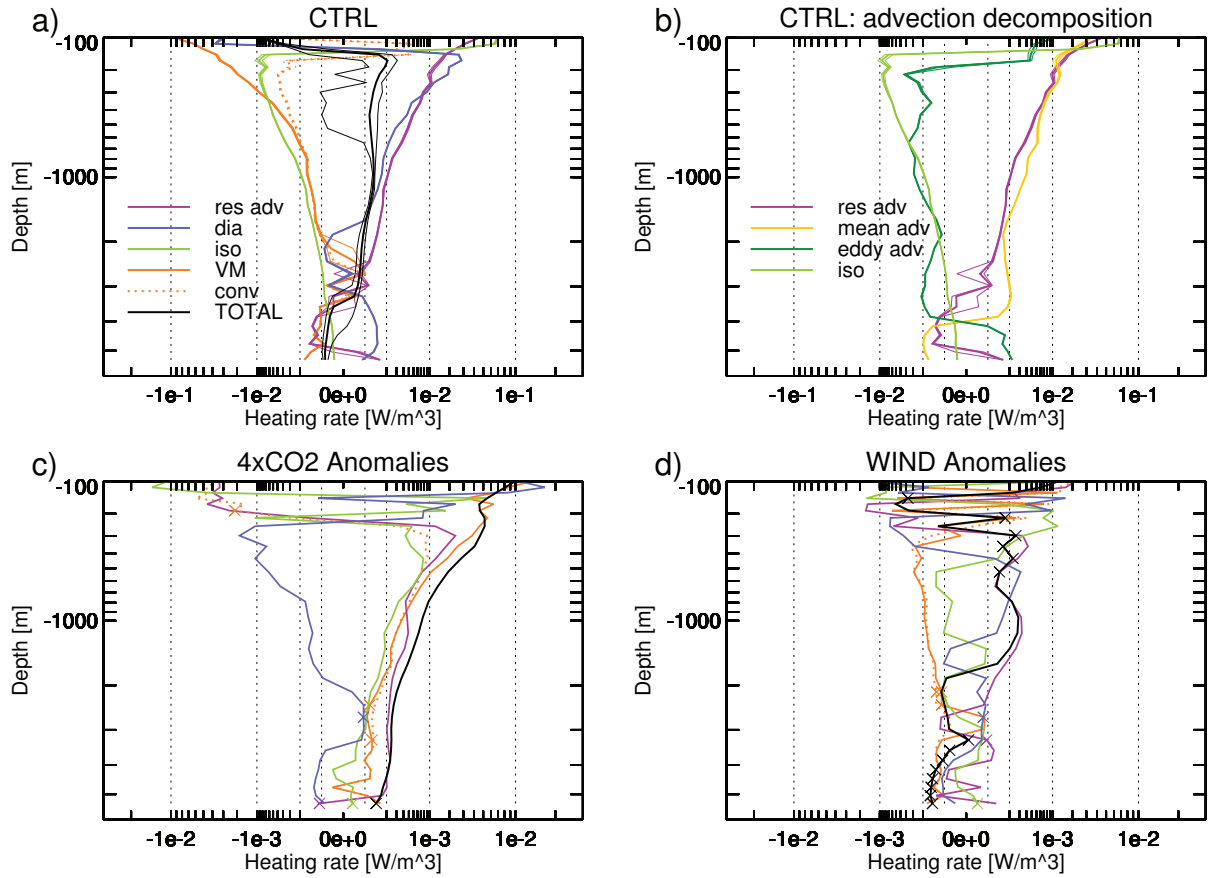


Fig. 3: The temperature tendency diagnostics as a function of depth in HiGEM1.2. Bold lines show a 70-year average from the control run and 20-year averages from the perturbation runs. The thin lines indicate a ± 1 standard deviation interval for the control run (CTRL). They are shown for the components as well as the total, but are hardly discernible since the standard deviation is relatively small in all of the cases. Both axes are stretched according to a power law to visualize both the large values in the mixed layer and the small values at depth. Dotted black vertical lines mark orders of magnitude. (a) CTRL, (b) decomposition of advective temperature change in CTRL, (c) 4xCO₂ minus CTRL, (d) WIND minus CTRL. Note the differing scale on the x-axis for panels (c) and (d). The individual processes are described in section 2.2. The abbreviations in the legend are “res adv” for residual advection, “dia” for diapycnal mixing, “iso” for isopycnal mixing, “VM” for vertical mixing (the sum of convection, “conv”, and mixed-layer physics), “mean adv” for mean advection and “eddy adv” for eddy advection. The crosses denote non-significant data points as explained in the text.

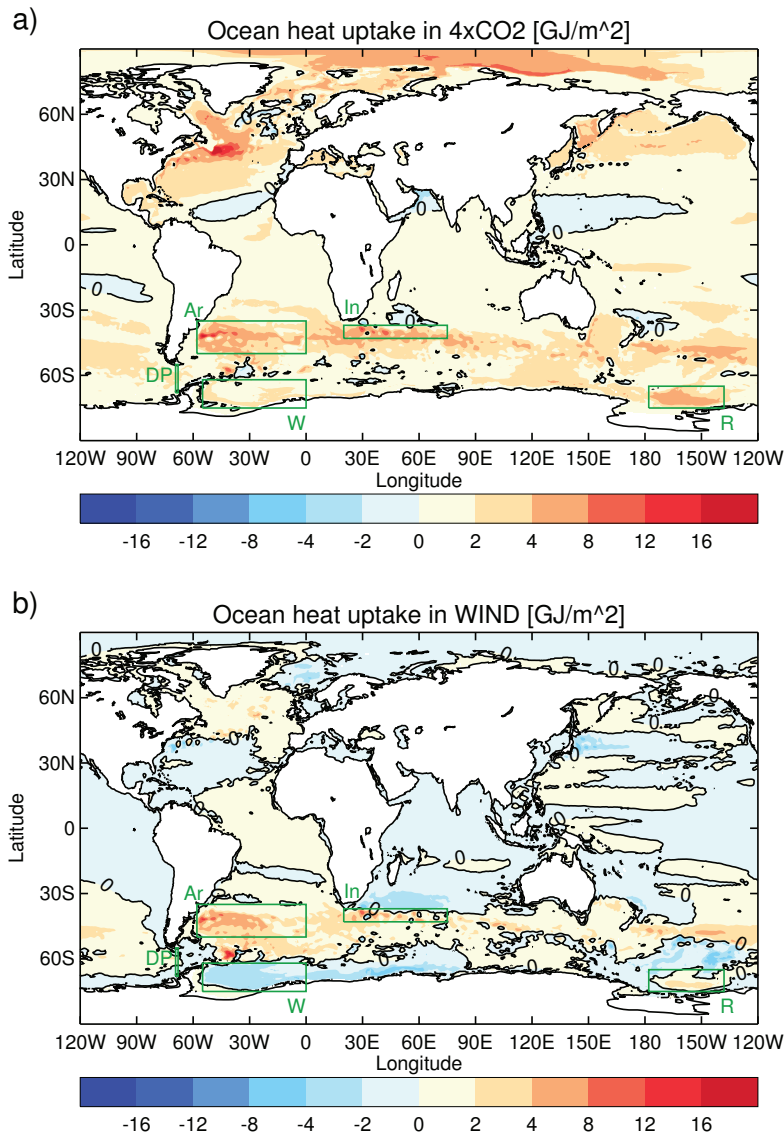


Fig. 4: Ocean heat uptake on the global average and averaged over the 20 years of the perturbation runs (a) 4xCO₂ and (b) WIND. The intervals of the colour scale are not constant. Green rectangles, marked with letters, show the regions of special interest. These are, in the Southern Hemisphere, from left to right: Drake Passage (DP), Argentine Basin (Ar), Weddell Gyre (W), Southwest Indian Ocean (In) and Ross Gyre (R).

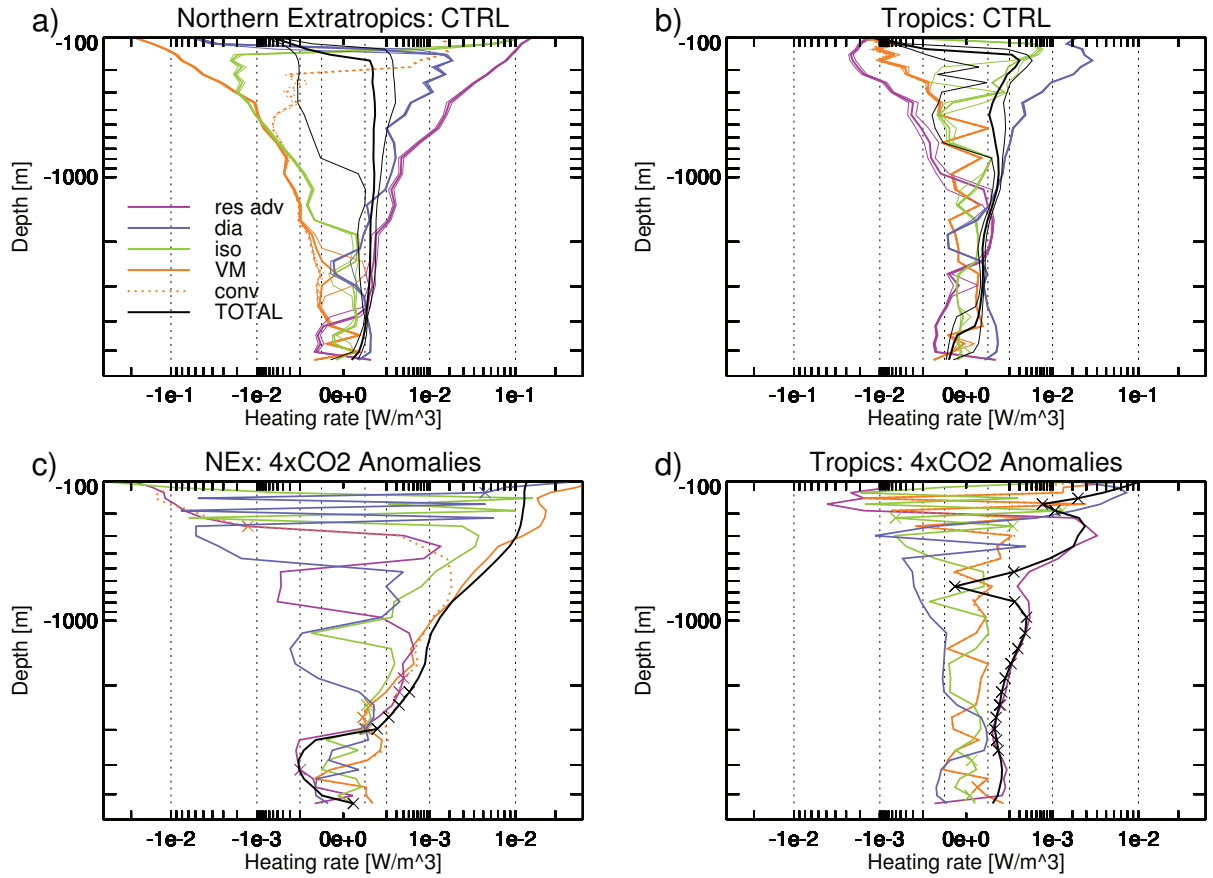


Fig. 5: Horizontally averaged temperature tendency diagnostics for (a) the control run in the Northern Extratropics region, (b) the control runs in the Tropics region, and the 4xCO₂ anomalies in (c) the Northern Extratropics and (d) the Tropics region. Both axes are stretched according to a power law to visualize both the large values in the mixed layer and the small values at depth. The dotted vertical lines denote orders of magnitude. Note the varying scales on the x-axis. Bold lines give the actual values, and thin lines (in the control run plots) indicate a ± 1 standard deviation interval. The standard deviations are shown for the components as well as the total, but are hardly discernible since the standard deviation is relatively small in all of the cases. See sec. 4 and Fig. 4 for the definition of the regions. For the abbreviations in the legend, see caption of Fig.3. The crosses denote non-significant data points as explained in the text.

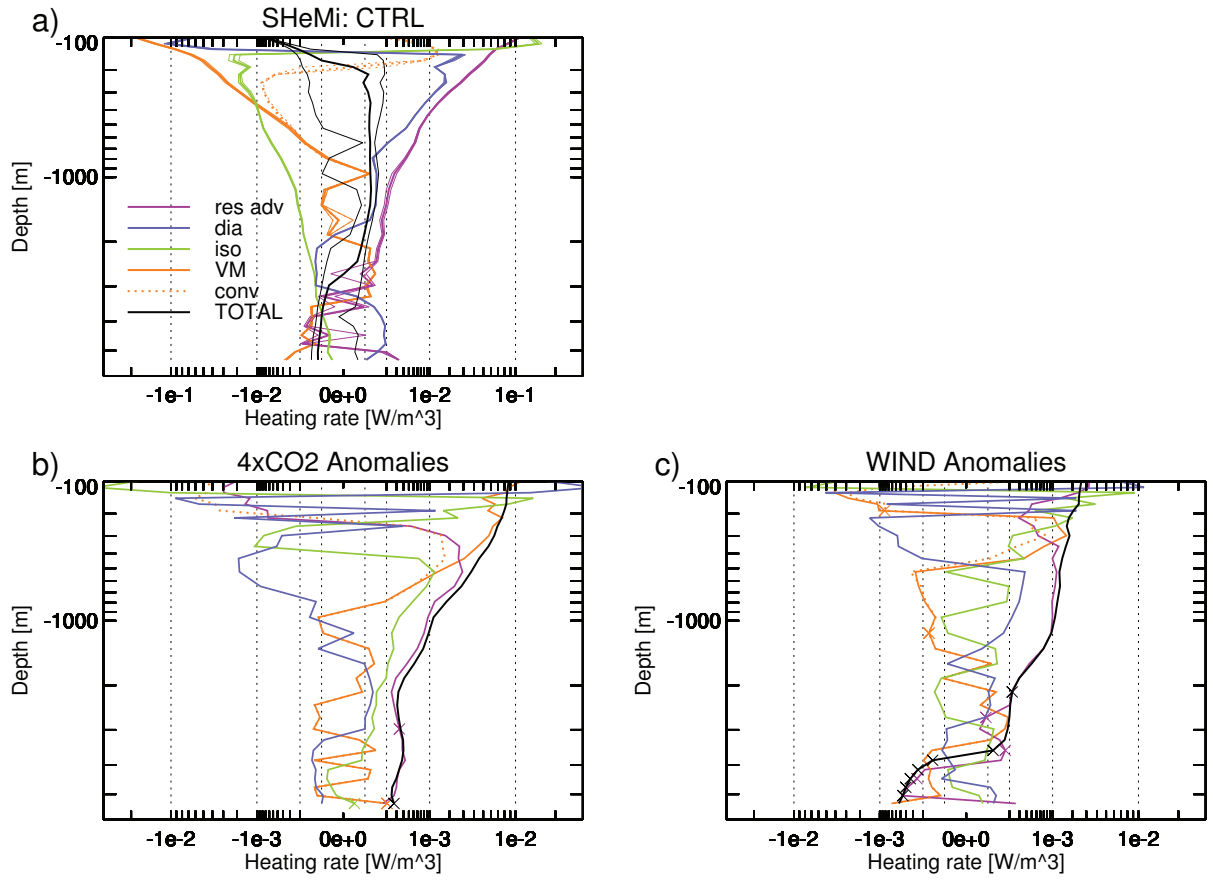


Fig. 6: Horizontally averaged temperature tendency diagnostics for the Southern Hemisphere mid-latitudes for (a) the control run, (b) the 4xCO₂ anomalies and (c) the WIND anomalies. Otherwise as Fig. 5.

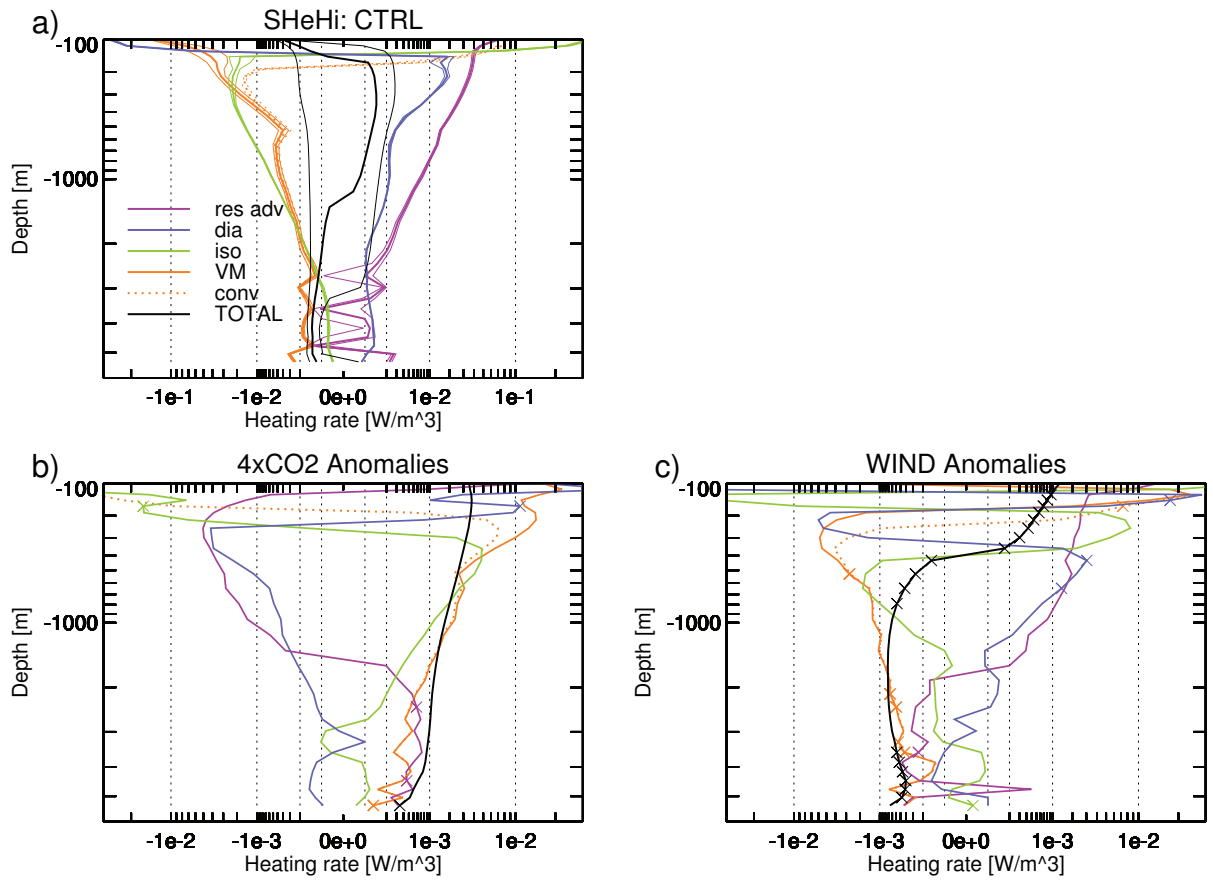


Fig. 7: Horizontally averaged temperature tendency diagnostics for the Southern Hemisphere high latitudes for (a) the control run, (b) the 4xCO₂ anomalies and (c) the WIND anomalies. Otherwise as Fig. 5.

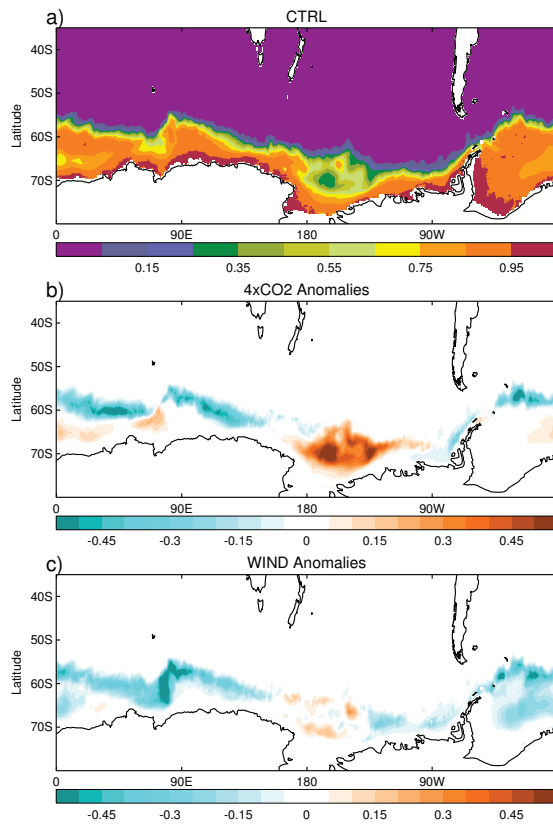


Fig. 8: September sea ice cover (in fractions) in (a) the control run, and anomalies of (b) 4xCO2 and (c) WIND.

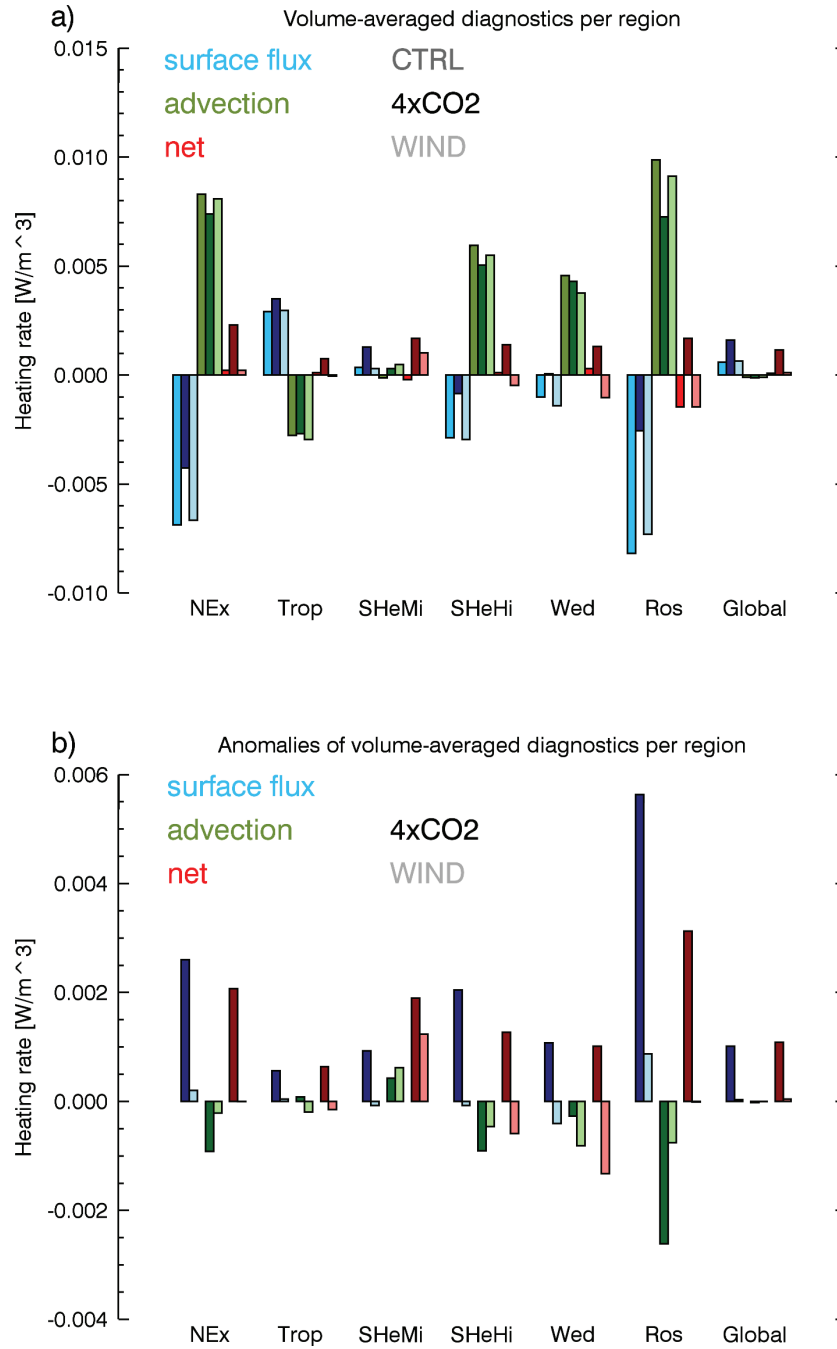


Fig. 9: Overview plot for the most relevant heat uptake processes in the regions of interest discussed in the text. The regions are defined in sec. 4. In (a), each region has three groups of three bars. Each group is colour coded according to the process it represents. In each group, the main colour comes in three hues, where the first bar is for CTRL, the second for 4xCO2 and the third for WIND. Each single bar gives the heating rate for a specific region, process and run. (b) shows the anomalies of the perturbation runs. Therefore, in each group, the main colour comes in two hues, where the first bar is for 4xCO2 (dark hue) and the second for WIND (light hue).

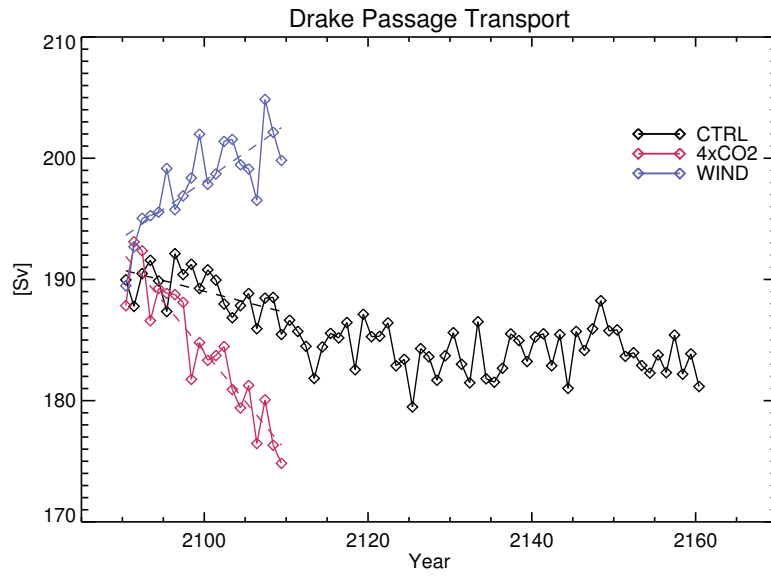


Fig. 10: Drake Passage transport in Sverdrup ($1 \text{ Sv} = 10^6 \text{ m}^3 \text{ s}^{-1}$) in the three HiGEM1.2 runs. Dashed lines: trend estimates over 20 years.

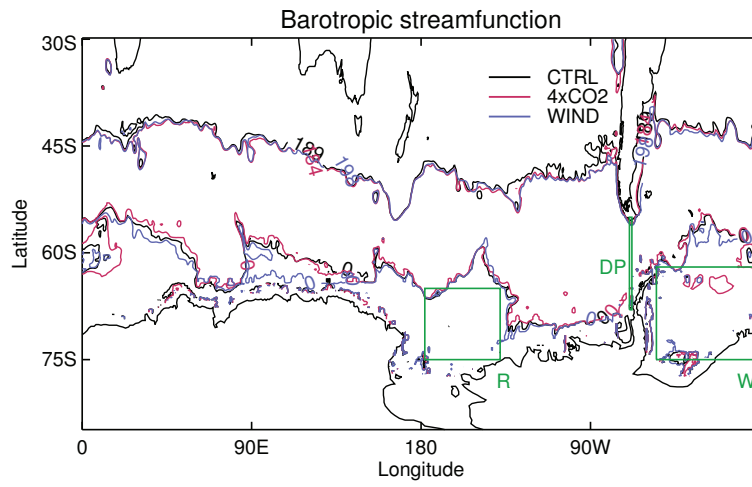


Fig. 11: Barotropic streamfunction contours (20-year average) in Sverdrup ($1 \text{ Sv} = 10^6 \text{ m}^3 \text{ s}^{-1}$) in the three HiGEM1.2 runs. Plotted are the minimum and maximum contours going through Drake Passage for each run. The minimum is 0 Sv by definition. The maxima are 189 Sv for CTRL, 184 Sv for 4xCO2 and 198 Sv for WIND. In addition, the -50 Sv contour has been plotted and shows, around 0°E and 60°S, the increase of the Weddell Gyre in 4xCO2.

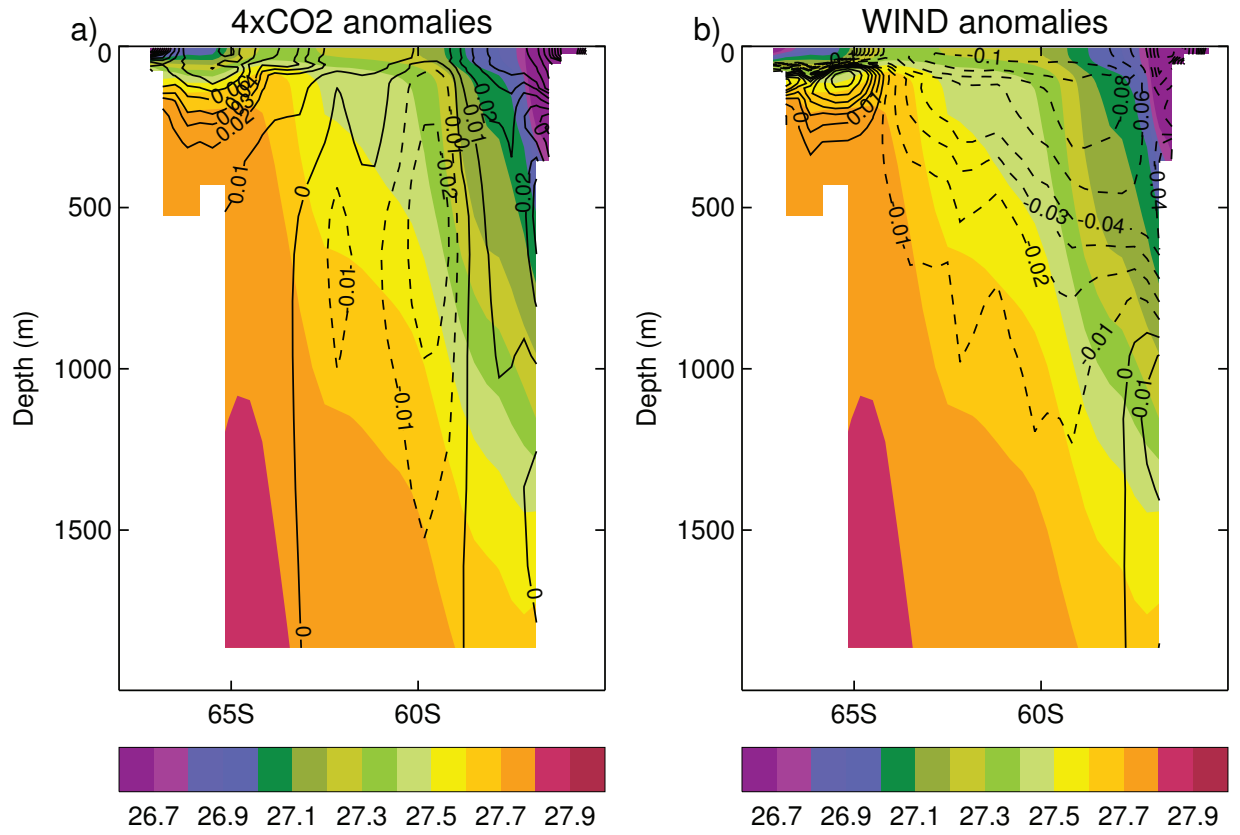


Fig. 12: Zonal average of potential density (shaded, in σ_2 units) and its anomaly (contours) in the Drake Passage region. (a) Anomalies of 4xCO₂, (b) anomalies of WIND. Solid contours indicate positive density anomalies and dashed contours indicate negative anomalies. In 4xCO₂ the isopycnals across the Drake Passage in the top ~1000 m flatten, while in WIND they steepen.

836 **References**

- 837 Banks HT, Gregory JM (2006) Mechanisms of ocean heat uptake in a coupled climate model
838 and the implications for tracer based predictions of ocean heat uptake. *Geophys Res Lett*
839 33:L07608, DOI 10.1029/2005GL025352
- 840 Bouttes N, Gregory J, Kuhlbrodt T, Suzuki T (2012) The effect of windstress change
841 on future sea level change in the Southern Ocean. *Geophys Res Lett* 39(23), DOI
842 10.1029/2012GL054207
- 843 Brierley CM, Collins M, Thorpe AJ (2010) The impact of perturbations to ocean-model
844 parameters on climate and climate change in a coupled model. *Clim Dyn* 34:325–343,
845 DOI 10.1007/s00382-008-0486-3
- 846 Cai W, Cowan T, Godfrey S, Wijffels S (2010) Simulations of processes associated with
847 the fast warming rate of the southern midlatitude ocean. *J Clim* 23:197–206, DOI
848 10.1175/2009JCLI3081.1
- 849 Church JA, White NJ, Konikow LF, Domingues CM, Cogley JG, Rignot E, Gregory JM,
850 van den Broeke MR, Monaghan AJ, Velicogna I (2011) Revisiting the Earth's sea-
851 level and energy budgets from 1961 to 2008. *Geophys Res Lett* 38:L18601, DOI
852 10.1029/2011GL048794
- 853 Downes S, Hogg A (2013) Southern Ocean circulation and eddy compensation in CMIP5
854 models. *J Clim* 26:7198–7220, DOI 10.1175/JCLI-D-12-00504.1
- 855 Dufresne JL, Bony S (2008) An assessment of the primary sources of spread of global
856 warming estimates from coupled atmosphere-ocean models. *J Clim* 21(19):5135–5144,
857 DOI 10.1175/2008JCLI2239.1
- 858 Eden C, Greatbatch RJ (2009) A diagnosis of isopycnal mixing by mesoscale eddies. *Ocean*
859 *Modelling* 27:98–106, DOI 10.1016/j.ocemod.2008.12.002
- 860 Exarchou E, Kuhlbrodt T, Gregory JM, Smith RS (2015) Ocean heat uptake processes: a
861 model intercomparison. *J Clim* 28(2):887–908, DOI 10.1175/JCLI-D-14-00235.1
- 862 Farneti R, Delworth TL, Rosati AJ, Griffies SM, Zeng F (2010) The role of mesoscale eddies
863 in the rectification of the Southern Ocean response to climate change. *J Phys Oceanogr*
864 40:1539–1557, DOI 10.1175/2010JPO4353.1
- 865 Frankcombe LM, Spence P, Hogg AM, England MH, Griffies SM (2013) Sea
866 level changes forced by Southern Ocean winds. *Geophys Res Lett* 40:1–6, DOI
867 10.1002/2013GL058104
- 868 Gent PR, McWilliams JC (1990) Isopycnal mixing in ocean circulation models. *J Phys*
869 *Oceanogr* 20:150–155
- 870 Gnanadesikan A, Slater R, Swathi PS, Vallis GK (2005) The energetics of ocean heat trans-
871 port. *J Clim* 18:2604–2616
- 872 Good P, Gregory JM, Lowe JA (2011) A step-response simple climate model to re-
873 construct and interpret AOGCM projections. *Geophys Res Lett* 38:L01703, DOI
874 10.1029/2010GL045208
- 875 Good P, Ingram W, Lambert FH, Lowe JA, Gregory JM, Webb MJ, Ringer MA, Wu P
876 (2012) A step-response approach for predicting and understanding non-linear precipita-
877 tion changes. *Clim Dyn* 39:2789–2803, DOI 10.1007/s00382-012-1571-1
- 878 Graham RM, de Boer AM, Heywood KJ, Chapman MR, Stevens DP (2012) Southern
879 Ocean fronts: Controlled by wind or topography? *J Geophys Res* 117:C08018, DOI
880 10.1029/2012JC007887
- 881 Gregory JM (2000) Vertical heat transports in the ocean and their effect on time-dependent
882 climate change. *Clim Dyn* 16(7):501–515, DOI 10.1007/s003820000059

- 883 Gregory JM, Forster PM (2008) Transient climate response estimated from radia-
884 tive forcing and observed temperature change. *J Geophys Res* 113:D23105, DOI
885 10.1029/2008JD014050
- 886 Griffies SM, Gnanadesikan A, Pacanowski RC, Larichev VD, Dukowicz JK, Smith RD
887 (1998) Isonutral diffusion in a z-coordinate ocean model. *J Phys Oceanogr* 28:805–830
- 888 Griffies SM, Winton M, Anderson WG, Benson R, Delworth TL, Dufour CO, Dunne JP,
889 Goddard P, Morrison AK, Rosati A, Wittenberg AT, Yin J, Zhang R (2015) Impacts on
890 ocean heat from transient mesoscale eddies in a hierarchy of climate models. *J Clim*
891 28(3):952–977, DOI 10.1175/JCLI-D-14-00353.1
- 892 Heuzé C, Heywood KJ, Stevens DP, Ridley JK (2013) Southern Ocean bottom water char-
893 acteristics in CMIP5 models. *Geophys Res Lett* 40:1–6, DOI 10.1002/grl.50287
- 894 Hieronymus M, Nycander J (2013) The budgets of heat and salinity in NEMO. *Ocean*
895 *Modelling* 67:28–38, DOI 10.1016/j.ocemod.2013.03.006
- 896 Huang B, Stone PH, Sokolov AP, Kamenkovich IV (2003a) The deep-ocean heat uptake in
897 transient climate change. *J Clim* 16:1352–1363
- 898 Huang B, Stone PH, Sokolov AP, Kamenkovich IV (2003b) Ocean heat uptake in transient
899 climate change: mechanisms and uncertainty due to subgrid-scale eddy mixing. *J Clim*
900 16:3344–3356
- 901 Kirkman IV CH, Bitz CM (2011) The effect of the sea ice freshwater flux on Southern
902 Ocean temperatures in CCSM3: deep-ocean warming and delayed surface warming. *J*
903 *Clim* DOI 10.1175/2010JCLI3625.1
- 904 Kuhlbrodt T, Gregory JM (2012) Ocean heat uptake and its consequences for the mag-
905 nitude of sea level rise and climate change. *Geophys Res Lett* 39:L18608, DOI
906 10.1029/2012GL052952
- 907 Large W, McWilliams J, Doney S (1994) Oceanic vertical mixing: A review and a model
908 with a nonlocal boundary layer parameterization. *Rev Geophys* 32(4):363–403, DOI
909 10.1029/94RG01872
- 910 Lee MM, Nurser AJG, Coward AC, de Cuevas BA (2007) Eddy advective and diffusive
911 transports of heat and salt in the Southern Ocean. *J Phys Oceanogr* 37:1376–1393, DOI
912 10.1175/JPO3057.1
- 913 Locarnini RA, Mishonov AV, Antonov JI, Boyer TP, Garcia HE, Baronova OK, Zweng
914 MM, Johnson DR (2006) *World Ocean Atlas 2009*. U.S. Government Printing Office,
915 Washington, D.C., US, NOAA Atlas NESDIS 68, vol 1, p 184
- 916 Manabe S, Bryan K, Spelman M (1990) Transient response of a global ocean-atmosphere
917 model to a doubling of atmospheric carbon dioxide. *J Phys Oceanogr* 20:722–749
- 918 Marshall J, Radko T (2003) Residual-mean solution for the Antarctic Circumpolar Current
919 and its associated overturning circulation. *J Phys Oceanogr* 33:2341–2354
- 920 Mazloff M, Heimbach P, Wunsch C (2010) An eddy-permitting Southern Ocean state esti-
921 mate. *J Phys Oceanogr* 40:880–899
- 922 Megann A, Storkey D, Aksenov Y, Alderson S, Calvert D, Graham T, Hyder P, Siddorn J,
923 Sinha B (2014) GO5.0: the joint NERC/Met Office NEMO global ocean model for use in
924 coupled and forced applications. *Geoscientific Model Development* 7:1069–1092, DOI
925 10.5194/gmd-7-1069-2014
- 926 Meijers A, Shuckburgh E, Bruneau N, Sallee JB, Bracegirdle T, Wang Z (2012)
927 Representation of the Antarctic Circumpolar Current in the CMIP5 climate models
928 and future changes under warming scenarios. *J Geophys Res* 117:C12008, DOI
929 10.1029/2012JC008412
- 930 Morrison AK, Saenko OA, Hogg AM, Spence P (2013) The role of vertical eddy transport
931 in Southern Ocean heat uptake. *Geophys Res Lett* 40, DOI 10.1002/2013GL057706

- 932 Munk W, Wunsch C (1998) Abyssal recipes II: energetics of tidal and wind mixing. *Deep-*
933 *Sea Research I* 45:1977–2010
- 934 Pardaens AK, Gregory JM, Lowe JA (2011) A model study of factors influencing projected
935 changes in regional sea level over the 21st century. *Clim Dyn* 36(9-10):2015–2033, DOI
936 10.1007/s00382-009-0738-x
- 937 Peters H, Gregg MC, Sanford TB (1995) Detail and scaling of turbulent overturns
938 in the Pacific equatorial undercurrent. *J Geophys Res* 100(C9):18,349–18,368, DOI
939 10.1029/95JC01360
- 940 Rahmstorf S (1993) A fast and complete convection scheme for ocean models. *Ocean Mod-*
941 *elling* 101:9–11
- 942 Roberts MJ, Marshall D (1998) Do we require adiabatic dissipation schemes in eddy-
943 resolving ocean models? *J Phys Oceanogr* 28:2050–2063
- 944 Sen Gupta A, Muir LC, Brown JN, Phipps SJ, Durack PJ, Monselesan D, Wijffels SE
945 (2012) Climate drift in the CMIP3 models. *J Clim* 25:4621–4640, DOI 10.1175/JCLI-
946 D-11-00321.1
- 947 Shaffrey LC, Stevens I, Norton WA, Roberts MJ, Vidale PL, Harle JD, Jrrar A, Stevens
948 DP, Woodage MJ, Demory ME, Donners J, Clark DB, Clayton A, Cole JW, Wilson SS,
949 Connolley WM, Davies TM, Iwi AM, Johns TC, King JC, New AL, Slingo JM, Slingo
950 A, Steenman-Clark L, Martin GM (2009) U.K. HiGEM: The new U.K. high-resolution
951 global environment model—Model description and basic evaluation. *J Clim* 22:1861–
952 1896, DOI 10.1175/2008JCLI2508.1
- 953 Sigmond M, Reader MC, Fyfe JC, Gillett NP (2011) Drivers of past and future Southern
954 Ocean change: stratospheric ozone versus greenhouse gas impacts. *Geophys Res Lett*
955 38:L12601, DOI 10.1029/2011GL047120
- 956 Wang Z, Kuhlbrodt T, Meredith MP (2011) On the response of the Antarctic Circumpolar
957 Current transport to climate change in coupled climate models. *J Geophys Res*
958 116:C08011, DOI 10.1029/2010JC006757
- 959 Wolfe CL, Cessi P, McClean JL, Maltrud ME (2008) Vertical heat transport in eddying ocean
960 models. *Geophys Res Lett* 35:L23605, DOI 10.1029/2008GL036138
- 961 Yin J (2012) Century to multi-century sea level rise projections from CMIP5 models. *Geo-*
962 *phys Res Lett* 39(17), DOI 10.1029/2012GL052947
- 963 Yin J, Griffies SM, Stouffer RJ (2010) Spatial variability of sea level rise in twenty-first
964 century projections. *J Clim* 23:4585–4607